NORTH WEST UNIVERSITY
A33641200162942C

THE RELATIVE BIOLOGICAL EFFECTIVENESS (RBE) OF A 200-MeV CLINICAL PROTON BEAM

TIMOTHY TIMO SEBEELA

THE RELATIVE BIOLOGICAL EFFECTIVENESS (RBE) OF A 200-MeV CLINICAL PROTON BEAM

TIMOTHY TIMO SEBEELA

A DISSERTATION SUBMITTED IN PARTIAL FULFILLMENT OF THE REQUIREMENTS FOR THE DEGREE OF MASTER OF SCIENCE IN APPLIED RADIATION SCIENCE AND TECHNOLOGY AT THE UNIVERSITY OF NORTH-WEST.

SUPERVISOR: Dr J.P SLABBERT
(iThemba LABS, Faure)

DECEMBER 2003

b1546773
LIBRARY
MAFIKENG CAMPUS
Call No.: TH 539.72 SEB
2005 -05- 19
Acc. No.: 051066
NORTH-WEST UNIVERSITY
1184306 61

ABSTRACT

Cancer therapy with high-energy particles has proved to be beneficial over the last 10 years. Protons are regarded as being more advantageous because of their distinctive physical depth dose distribution that allows dose conformation to the tumor while sparing normal tissue. In this study, the relative biological effectiveness (RBE) values for the 200-MeV clinical proton beam at iThemba LABS were measured at strategic positions along a 5 cm Spread-Out-Bragg-Peak (SOBP).

RBE values were evaluated at the initial plateau of the virgin beam (24.2 mm in Perspex), and at the middle part, distal part and distal edge (12.4% max. dose) along the SOBP (depth in Perspex = 161.4, 181.3 and 207.7 mm respectively). Biological systems used were Chinese hamster ovary cells (CHO-K1) for both cell survival and micronuclei frequencies as well as human T-lymphocytes for micronuclei frequency analysis. ^{60}Co γ-irradiation served as a reference.

Cell survival measurements yielded RBE values of 1.17 at the distal part and 1.62 at the distal edge (12.4 max. dose). For micronuclei analysis, a limiting $RBE_{\alpha p+/\alpha\gamma}$ value of 1.3 at the distal part was observed. Using T-lymphocytes, $RBE_{\alpha p+/\alpha\gamma}$ values calculated were 2.1, 2.7 and 3.2 at the middle part, distal part and distal edge, respectively.

These results show an increase in RBE with depth of penetration and are explained by an increase in ionization density at the end of the SOBP. This is influenced by a high fraction of low-energy protons at that position. Protons were found to be most potent per unit dose towards the end as they slow down to a complete stop. It is recommended that an RBE value slightly greater than the current 1.1 be applied in therapy. Also, that the less steep biological effective depth dose curve be taken into account when dose planning.

ACKNOWLEDGEMENTS

Working jointly with Dr JP Slabbert as my supervisor has been a rewarding experience. His guidance, persistence and expertise in the field were invaluable towards the success of this research and dissertation.

Mr. S Maage, S Bakhane and J Symons for beam control during measurements.

iThemba LABS and the North West University for giving me the chance to endeavour into the world of Nuclear Technology.

My sister Susan Sebeela for her support and audacity since the beginning of my studies.

"I give thanks to God who has given me strength for my work"

1Timothy 1 vs 12

His love and guidance has shown me that nothing is impossible, even under extraordinary circumstances.

TABLE OF CONTENTS

Abstract.....II

Acknowledgements.....III

Table of Contents.....IV

List of Abbreviations.....VI

List of Figures.....VII

List of Tables.....XI

CHAPTER 1: Research Problem

1.1 Introduction.....1

1.2 Stopping Powers and Energy variation for Protons.....3

1.3 Ionization Density and Biological Effectiveness.....5

1.4 Fractionation Treatments and Radiation Quality.....6

1.5 Radiation Quality and the Spread Out Bragg Peak.....8

1.6 Purpose of this Investigation.....10

1.7 The iThemba LABS Proton Therapy Facility.....12

CHAPTER 2: Literature Review

2.1 Radiotoxicity of Protons on Cells.....15

2.2 RBE and LET relationship.....18

2.3 RBE variations with Biological Parameters.....22

CHAPTER 3: Research Materials and Methods

3.1 Cell Storage, Retrieval and Culture Maintenance.....30

3.2 CHO-K1 Cell Preparation for Survival Analysis.....32

3.3 Staining and Counting of Colonies.....33

3.4 CHO-K1 Cell preparation for Micronuclei Analysis.....33

3.5 Isolation of T-lymphocytes from Whole-blood.....35

3.6 T-lymphocyte Preparation and Staining for Micronuclei Analysis.....36

3.7 Proton Irradiation and Dosimetry.....38

3.8 ^{60}Co γ- Irradiation and Dosimetry.....41

CHAPTER 4: Results and Discussions

4.1 Test of CHO-K1 Viability when left without Medium.....42

4.2 Survival of CHO-K1 cells after Proton Irradiation.....45

4.3 Confidence Ellipses for Cell Inactivation Parameters.....51

4.4 Usefulness of Micronuclei in CHO-K1 cells to reflect Cellular damage.....53

4.5 Micronuclei frequencies in CHO-K1 cells in Response to Protons.....56

4.6 Confidence Ellipses of Micronuclei Frequency Response Curves.....61

4.7 Micronuclei Frequencies in T-lymphocytes.....62

4.9 Confidence Levels of Micronuclei Frequencies in T-lymphocytes.....73

4.8 RBE variations with Dose.....75

CHAPTER 5: Conclusions and Recommendations

5.1 Conclusions and Recommendations.....77

List of Abbreviations

RBE – Relative Biological Effectiveness

SOBP – Spread-out-Bragg-peak

LET – Linear energy transfer

CHO-K1 – Chinese hamster ovary cells

α-MEM – alpha-Minimum essential medium

RPMI – Roswell park memorial institute

PBS – Phosphate buffered saline

DMSO – Dimethyl-Sulphoxide

Gy – Gray (S.I. unit for radiation dose)

MeV – Mega electron volts

keV – kilo electron volts

rpm – revolutions per minute

ml – milliliter

μg – micro-gram

List of Figures

Fig 1.1.1. A schematic showing a Relative dose in tissue or water against depth for heavy ion beams [Fowler 1981].

Fig 1.2.1. The change in stopping powers as a function of energy measured in water.

Fig 1.6.1. The depth dose profile of a 5 cm Spread Out Bragg Peak generated at iThemba LABS, Faure and depicting the relative low entrance dose, high dose in the peak region and sharp dose reduction in the distal edge. Arrows indicates the positions where the cells were placed when doing measurements.

Fig 1.7.1. Layout of the 200 MeV horizontal proton therapy beam modification system. The drawing is not to scale, but all the beam line components are shown in their approximate positions. [http://www.tlabs.ac.za/public/MedicalRadiation(Protons).htm]

Fig 1.7.2. A 5cm range modulating wheel (Propeller), made of acrylic, is used to spread out the Bragg peak of the proton beam.

Fig 2.1.1. The direct and indirect actions of radiation with the DNA of the cell, the letters S, P, A,T, G and C represents sugar, phosphorus, adenine, thymine, guanine and cytosine, respectively. [Hall 2000].

Fig 2.2.1. Generalized relationship between RBE and LET [IAEA Manual 2001].

Fig 2.2.2. Schematic representation based on experimental data the relationship between RBE and LET for protons, α-particles and heavy ions [Raju M.R 1995].

Fig 2.2.3. Microdosimetric spectra measured at different depths in the 85 MeV proton beam produced at Louvain-la-Neuve, and for ^{60}Co γ-rays. The biological weighting function r(y) for intestinal crypt regeneration has been superimposed. This function expresses the variation of RBE as a function of linear energy (y) [Gueulette et al., 1996].

Fig 3.2.1. A schematic flow diagram showing how the cells were diluted in test tubes and then seeded in petri dishes before being irradiated. Numbers in brackets represents cell suspension volumes while the others represent that of the growth medium.

Fig 3.6.1. An example of a binucleated T-lymphocyte with two micronuclei resulting from exposure to ionizing radiation.

Fig 3.7.1. Experimental setup using syringes to irradiate the cells, a thick block of Perspex used as a backscatter was placed behind the syringes during the treatment.

Fig 3.7.2. Proton experimental setup using petri dishes to irradiate a monolayer of cells. An arrow shows the position of the petri dish during the treatment.

Fig 3.7.3. A 200 MeV proton beam response with depth of penetration in blocks of Perspex for the 5cm SOBP and the virgin beam.

Fig 3.7.4. A Markus chamber placed at the position of irradiation to monitor the beam delivery, a thick block of Perspex serving as a backscatter was placed closely at the back of the chamber during the measurements.

Fig 4.2.1. An example of colonies formed after proton irradiation. In column A 200 cells were seeded and 138 survived. In columns B, C and D 4000 cells seeded were and a dose of 6 Gy given in the plateau (B), distal part of the SOBP (C) and at the distal edge with 12.4 % dose of maximum (D).

Fig 4.2.3. Survival fraction curves of CHO-K1 cells exposed to protons at different positions along the SOBP. Cells were irradiated at the Plateau (■), distal part (▲) and the distal edge (▼). Error bars indicate standard deviations.

Fig 4.3.1. 95% confidence ellipses of survival data for CHO cells exposed to 200 MeV protons at different positions in the SOBP. Symbols in the middle of the ellipses indicate the best for fit the respective survival curves.

Fig 4.4.1 Surviving fractions of CHO-K1 cells exposed to gamma radiation ranging between 1 and 5 Gy and plotted as a function of micronuclei frequencies observed in each instance.

Fig 4.4.2 Surviving fractions of CHO-K1 cells exposed to p(66)/Be neutrons ranging between 0.5 and 2.5 Gy and plotted as a function of micronuclei frequencies observed in each instance.

Fig 4.5.1. Percentages of the CHO-K1 cells that are binucleated for different samples irradiated in the plateau (▼) and in the distal part (●) of the SOBP.

Fig 4.5.4. Dose response curve of the micronuclei frequencies observed per 500 binucleated CHO-K1 cells. Positions of treatment were the plateau (▲) of the virgin beam and distal edge (■) of the SOBP.

Fig 4.6.1. 95 % confidence level of the cells micronuclei frequency data for CHO-K1 cells, following exposure in the plateau region and distal portion of the SOBP of a 200 MeV proton beam.

Fig 4.7.1. Nucleation indices for T-lymphocytes in response to dose absorbed at different positions in a 200 MeV proton Bragg curve. Included are also data for exposure to ^{60}Co γ-rays.

Fig 4.7.8. Dose response curves of the micronuclei frequency observed per 500 binucleated T-lymphocytes. Positions of irradiation were in the Plateau (♦) and Distal Edge (■) of the virgin beam. Position of irradiation were in the Middle (▼), Distal Part (▼) and Distal Edge (X) for the SOBP. ^{60}Co γ-irradiation (▲) is included, as well.

Fig 4.8.1. 95% confidence ellipses of the dose response parameters that describe the formation of micronuclei in lymphocytes.

Fig 4.9.1. RBE response per unit dose of protons absorbed at different positions along the SOBP.

List of Tables

Table 4.1.1. Plating efficiency of CHO-K1 cells defining cell viability after monolayers had been left with out growth medium for different time intervals. The data is compared to that of a control set of cultures.

Table 4.1.2. Binucleation levels as a function of the time for CHO-K1 cells left without growth medium.

Table 4.2.2. The mean survival fractions and their standard deviations for CHO-K1 cells irradiated in the plateau region of the unmodulated beam (24.2 mm Perspex), distal part of the SOBP (181.3 mm Perspex) and at the distal edge (207.7 mm Perspex) corresponding to 12.4 % of the dose at maximum.

Table 4.2.4. Survival curve parameters for CHO-K1 cells irradiated at different positions along the SOBP. The RBE is also indicated.

Table 4.2.5. Comparison of previous RBE measurements with different initial beam energies for different cell and tissues types and position along the SOBP.

Table 4.5.2. Micronuclei frequency observations in binucleated CHO-K1 cells and their respective binucleation levels after exposure to protons in the plateau region.

Table 4.5.3. Micronuclei frequency observations in binucleated CHO-K1 cells and their respective binucleation levels after exposure to protons in the distal part of the SOBP.

Table 4.5.5. Mean dispersion index (σ^2/y) and mean standard unit normal deviation (μ) for micronuclei frequencies in CHO-K1 cells.

Table 4.7.2. Micronuclei frequency distributions observed in binucleated T-lymphocytes exposed to ^{60}Co γ-irradiation.

Table 4.7.3. Micronuclei frequency distributions observed in binucleated T-lymphocytes exposed to protons in the plateau region of the unmodulated beam.

Table 4.7.4. Micronuclei frequency distributions observed in binucleated T-lymphocytes exposed to protons in the middle part of the SOBP.

Table 4.7.5. Micronuclei frequency distributions observed in binucleated T-lymphocytes exposed to protons in the Distal Part of the SOBP.

Table 4.7.6. Micronuclei frequency distributions observed in binucleated T-lymphocytes exposed to protons in the distal edge (12.4% max. dose) of the SOBP.

Table 4.7.7. Micronuclei frequency distributions observed in binucleated T-lymphocytes exposed to protons in the distal edge (12.4% max. dose) of the virgin beam.

Table 4.7.9. Lymphocyte micronuclei frequency parameters and their calculated RBE values at different positions along the SOBP.

Table 4.7.10. Mean dispersion indices (σ^2/y) and mean standard unit normal deviations (μ) for micronuclei frequencies in T-lymphocytes at different positions.

NWU LIBRARY

CHAPTER 1

1. RESEARCH PROBLEM

1.1 Introduction

The first Proton therapy patient was treated at Faure on the 10 September 1993 using a horizontal 200-MeV beam. This event marked the use of protons for therapy by only the fifth Institution in the world and the only one in the Southern Hemisphere, and follows the very first use of high-energy protons initiated at Uppsala (Sweden) in 1957. At first, patients were treated at Faure with a so-called shoot-through protocol where irradiations were performed using only the plateau region of the beam. Although crossfire treatment plans were used, the physical characteristics of the proton beam, when its use is constrained to this protocol, is very similar to that of ^{60}Co γ-rays and, as such, the radiobiology of the protons in use is not different from that of most conventional radiotherapy sources [Slabbert *et al.*, 1994]. By contrast, a treatment with a Spread-Out-Bragg-Peak (SOBP), first given on 18 February 1994 [NAC/AR 1994], and with such an application the radiotoxicity of the proton beam is expected to vary. The radiobiological findings reported here deal mainly with the potency of protons when administered as a SOBP.

The objective of cancer treatment with high-energy particles is to eradicate the tumour while sparing normal tissue. Radiotherapists have been attracted to proton beams due to the clinical advantages that arise as a result of the distinctive depth dose distribution of these charged particles along the Bragg curve. This starts with a low dose entrance in the plateau region (absorbed by normal tissues) and is followed by high doses of radiation

that can be positioned in the target volume. Furthermore, the Bragg curve ends with a very sharp dose reduction at the distal edge. This depth dose profile makes it most suitable to treat lesions as the radiation energy absorbed by deep-seated tumours can be very high, and at the same time the dose to sensitive structures is restricted.

The absence of radiation dose distal to the treatment volume allows one to re-treat patients when the disease re-occurs in close proximity to the original site, without fear of delivering more than the tolerance dose to sensitive normal tissue. For example, re-occurrence of lung cancer when the treatment plan inevitably involves exposure of the spinal cord.

These advantages are unique to charged particles and depth dose characteristics are very different from that of non-charged radiation modalities like X-rays and neutrons (Fig 1.1.1). Carbon and other ions, such as helium and neon, although much heavier than protons also have such favourable depth dose characteristics [Fowler 1981]

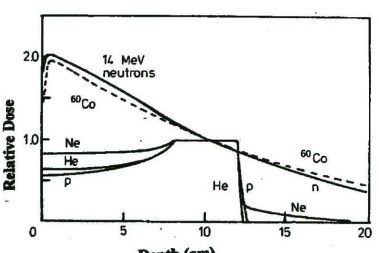


Fig 1.1.1. A schematic showing a relative dose in tissue or water against depth for heavy ion beams [Fowler 1981].

An important characteristic of radiation energy absorbed in tissue from charged particles is that not only does the macroscopic dose along the Bragg curve vary, but that a change in the microscopic dose can also be expected with depth. This is mainly due to particles losing energy at depth and as such a unit dose of radiation energy absorbed has an increased ionization density as protons slow down. For this reason, a change in the relative biological effectiveness (RBE) of protons is anticipated.

Physical depth dose profiles can be measured in a few minutes, with relative ease using ionization chambers and other types of dosimeters [Jones 2000]. This is most important to ensure accurate radiotherapy and optimal planning protocols. Knowing the macroscopic physical dose with great precision is however not enough to reflect in full the biological damage induced by a unit dose of radiation energy. In order to understand the therapeutic impact of protons it is essential to also quantify the relative biological effectiveness of a known physical dose of protons and compare that with the radiotoxicity of a reference radiation. This can only be done using suitable biological endpoints requiring time-consuming methodologies. The principle purpose behind this investigation is to follow the RBE of the 200 MeV proton beam used for radiotherapy at iThemba LABS.

1.2 Stopping power and energy variation for protons.

Looking at the depth dose profile for protons (Fig. 1.6.1), it is apparent that protons lose energy as they enter tissue and continue to do so, at different rates, along the Bragg curve. As the proton dose becomes zero at some depth, it implies that protons have

decelerated from their initial high energies to a complete stop. As the ionization density for a particular radiation type is inversely proportional to energy, the linear energy transfer for protons can be expected to be different along the Bragg curve. The magnitude of change can be appreciated by considering the change in stopping powers for protons as a function of energy [ICRU Report 49]. For example, in water the stopping power for protons at 200 MeV is about 5 $MeV.cm^2.g^{-1}$ and increase to some 900 $MeV.cm^2.g^{-1}$ for protons with energy of 0.1 MeV. Interestingly, the ration of stopping powers is approximately the same irrespective of the initial proton energy [Laitano and Rosetti 2000].

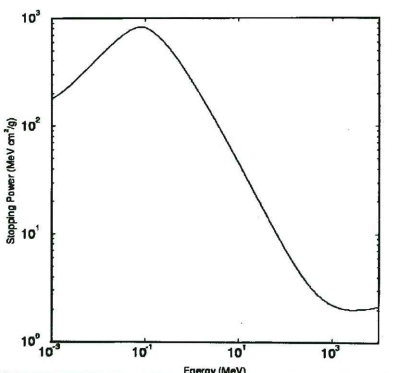


Fig 1.2.1. The change in stopping powers as a function of energy measured in water.

From this it follows that considerable changes in the ionization density of proton therapy beams can be expected. The latter determines, in part, the radiation quality [Chadwick and Leenhouts 1981] and this, in turn, the relative biological effectiveness of the treatment modality.

1.3 Ionization density and biological effectiveness.

Radiation modalities available for radiotherapy differ in ionization density and, as a result, in their relative biological effectiveness. This is because the mean linear energy transfer (LET) is different for different types of radiation. For example, a total dose of 20 Gy neutrons is considered to be iso-effective to 60 Gy of 6 MV X-rays. Although this implies an RBE of 3, the relative biological effectiveness of a particular radiation type is determined by many factors. This include physical factors, such as dose and ionization density, as well as biological parameters such as cell type, inherent radiosensitivity and physiological status, such as oxygen tension.

RBE is defined as the biological measurement to determine a dose (total dose or dose/fraction) of a new radiation (eg. Protons or Neutrons) required to produce the same clinical effect as a dose of a conventional radiation (eg. ^{60}Co γ-rays or X-rays). The ratio of the two doses (conventional/test radiation) is taken as the RBE value. [Wambersie *et al.*, 2002].

LET is the energy transferred per unit length of track and is measured in keV/μm [Hall 2000]. The distribution of LET along the length of clinical proton beam varies within the initial energy of the beam, the size of the SOBP and the position within the SOBP

because protons at the proximal position of SOBP are of higher energy and thus lower LET while at the distal position it composed of relatively large portion of lower energy and higher LET protons [Gueulette *et al.*, 1996].

The fact that different types of radiation have different relative efficiencies for the induction of a biological endpoint is one of the most interesting effects in radiation biology and one that has especially attracted the attention of radiation physicists. It has been concluded that when comparing the relative toxicity of various radiations, it is assumed that the comparison is on the basis of equal amounts of energy absorbed [Cember 1980]. Generally, the higher the rate of LET of the radiation, the more effective it is in damaging tissues.

1.4 Fractionation treatments and radiation quality

Proton therapy is usually associated with radiosurgery and hypofractionated stereotactic therapy (Vernimmen *et al.*, 2001). In these protocols treatment is given once and three or four times, respectively. Knowledge of changes in the RBE of a proton therapy beam with depth is in itself important to optimize such treatments. Moreover, variations in beam quality will have a bigger impact when treatment is given in a higher number ($n>4$) of fractions. This is happening more frequently in recent years, as more treatment centres are now available than ever before. A number of modern facilities have come online during the last 10 years and more are in a stage of planning [Skarsgard 1998]. These proton facilities use cyclotrons dedicated to therapy and, as such, allow particle treatment to be administered using an increasing number of fractions - approaching that used in

conventional treatment protocols. At one stage, no less than four therapy sessions have been available per week at iThemba LABS.

In principle, any increase in biological effect due to an in increase in ionization density is amplified when treatment is given in more fractions – i.e. lower doses per fraction are administered. For example, with fractionation neutron therapy the RBE increases with the number of fractions given [Hall and Brenner 1993]. The RBE for acute irradiation increases from 1.5 to 2.6 when compared to that for four fractions (Hall 2000). It is instructive to note that RBE variations due to a change in ionization density and different fraction schemes are mainly the result of a higher repair capacity for tissue exposed to the reference radiation. This phenomenon is most expressed when comparing high-LET neutrons with X-rays. Even so, the same principle will apply to protons of different energies.

The relative importance of changes in beam quality is further accentuated when one considers that proton therapy is often administered to brain lesions surrounded by normal tissue that have a very high capacity for repair. Also, some target tissues in the treatment of non-malignant lesions, like arterio-venous malformations and meningiomas have very strong capabilities to repair from radiation [Hall and Brenner 1993]. Therefore, it can be put forward that variations in proton RBE will be relatively more important for therapy of tissue types with low alpha / beta ratios. In fact, this conjecture is supported by high RBE values that related to low alpha/ beta ratios, by Gerweck and Kozin (1999).

Low alpha / beta ratios are associated with slow dividing tissue and so-called late effects. It is not surprising, therefore, that influence of fractionation on late effects has been considered by some investigators in their studies of clinical proton beams. Fractionated radiobiological studies have been performed to investigate proton toxicity at different positions along the Bragg curve for biological effects that developed over as much as one year, for example lung fibrosis [Gueulette *et al.*, 2000], and this is then compared to early responding tissue, eg. crypt stem cell regeneration [Gueulette *et al.*, 2001].

1.5 Radiation quality and the Spread Out Bragg Peak

Expected changes in ionization density of a clinical proton beam are not only the result of changes in proton energy, but modulation of the Bragg peak may also be of significance. The Bragg peaks of clinical proton beams are routinely modulated so as to extend the peak to position the maximum dose uniformly across the tumour volume. Although slower moving protons form the basis for any increase in RBE with depth, the inherent characteristics of an unmodulated and modulated proton beam are different. In particular, the dose absorbed in the distal edge of a Bragg peak is the result of different proton energy components dependent on the beam being modulated, or not.

In an unmodulated beam the distal edge comprises of proton energies lower than that in the plateau and this in itself may result in a higher ionization density. It is unclear if the reduction in proton energy in itself is of any biological importance as no data on this has been published to date. The lack of data from the distal edge of a virgin beam is not surprising as unmodulated proton beams are used only in shoot-through protocols. Since

the distal edge is outside the patient, its radiobiological characteristics have no clinical consequences. By contrast, the dose in the distal edge of a spread out Bragg peak (SOBP) is made up by protons of very different energies. This includes relatively low energy protons from a single unmodulated beam, and also very low energy protons form the distal edges of Bragg peaks that have been shifted upstream as result of modulation (see Fig 1.6.1). The latter makes a small contribution to the total dose absorbed but the question arises do these very low energy proton particles have any significant biological consequences? This aspect is, in part, the objective of this investigation.

A mixture of charged particles with different ionization densities is not unique to the distal edge of a modulated proton beam but is also characteristic of neutron radiation energy absorbed by cells [Wambersie 1996]. When looking at the microdosimetric distribution of charged particles induced by neutrons it becomes evident that only a small portion of the physical dose is the result of high-LET radiation and this stems mainly from α-particles and heavy recoil fragments. The bulk of the dose absorbed by cells is in fact by relative low-LET knock-on protons. Yet, the biological damage that follow neutron irradiations is distinctly different from that of low-LET radiation - this include the formation of less repairable damage and oxygen enhancement values lower than that for low-LET radiation sources. Considering that high-LET radiation, even when making only a small contribution to the total dose, has such a strong influence on biological outcome, it becomes conceivable that the mixture of charged particles in the distal edge of a proton beam may also induce biological damage akin to that of high-LET radiation.

1.6 Purpose of this investigation.

Optimal radiosurgery and fractionated stereotactic radiotherapy using such a particle beam is reliant on knowing the RBE of this treatment modality both with respect to other types of radiation as well as different types of tissues. Changes in the radiotoxicity of protons are investigated as the high-energy protons (200 MeV) entering the target tissue slow down towards the distal edge (Fig 1.6.1) resulting in an increase in the ionization density. The radiotoxicity of the beam is investigated at different positions along the SOBP (Fig 1.6.1) using cells in culture.

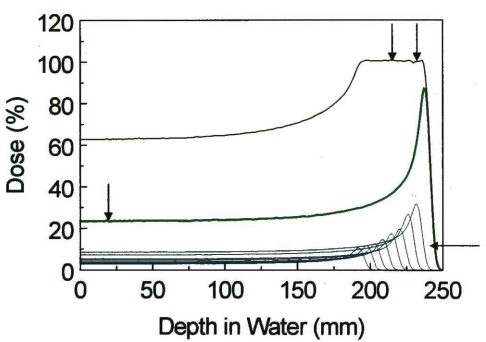


Fig 1.6.1. The depth dose profile of a 5 cm Spread Out Bragg Peak generated at iThemba LABS, Faure and depicting the relative low entrance dose, high dose in the peak region and sharp dose reduction in the distal edge. Arrows indicates the positions where the cells were placed when doing measurements.

It is very useful to quantify the RBE of the clinical proton beam at the very distal part of the SOBP. The last few millimeters of the SOBP are important as the dose absorbed is at a maximum whilst the protons are starting to slow down.

Also, the distal edge is of particular importance as lower energy protons can be expected to induce more biological damage in cells, even though the physical dose absorbed is the same, or reduced, compared to that when protons enter a patient. This means the biological effectiveness of the proton treatment will not be the same at various positions in the target volume (tumour) even though the physical dose remains constant. The net effect of this is that the treatment of the disease will also not be equal at different areas within the tumour. This can be corrected by modulating the beam in an appropriate manner, and for this the RBE of the proton beam at different depths needs to be quantified.

Due to the substantial increase in the clinical applications of proton beams, the uncertainties that lie within the RBE of this treatment modality need to be investigated in order to facilitate the comparison of clinical results obtained at different treatment centres.

1.7 The iThemba LABS proton therapy facility.

The clinical 200-MeV proton beam produced at iThemba LABS, Faure has fixed horizontal direction and is located next to the fast neutron irradiation facility. Protons are accelerated by a separated sector cyclotron combined with a solid pole injector cyclotron and exit the vacuum system with an energy of approximately 200 MeV. The beam is flattened with scatterers plus an occluding ring system made of brass, that also enlarges the beam diameter and maintains a uniform dose distribution. The maximum diameter of a useful beam is about 100mm at the treatment position. The total distance between the beam line vacuum window and the treatment isocenter is 7 m (Jones *et al.*, 2002).

A rotating wheel (modulator propeller) made of different thicknesses of acrylic is used to spread out the Bragg peak. The modulator propeller increasingly degrades the beam energy resulting in a series of plateaus and Bragg peaks of varying intensities that superimpose to produce a SOBP (Fig 1.6.1).

Since identical beam energies cannot be reproduced every day, plastic range trimmer plates, 0.6 mm, thick are placed immediately upstream of the modulator propeller in order to routinely produce a residual range of 24.00 ± 0.03 cm in water for patient treatment. This distance is defined to the distal edge at 50% level and corresponds to proton energy of 191 MeV.

The Proton beam line

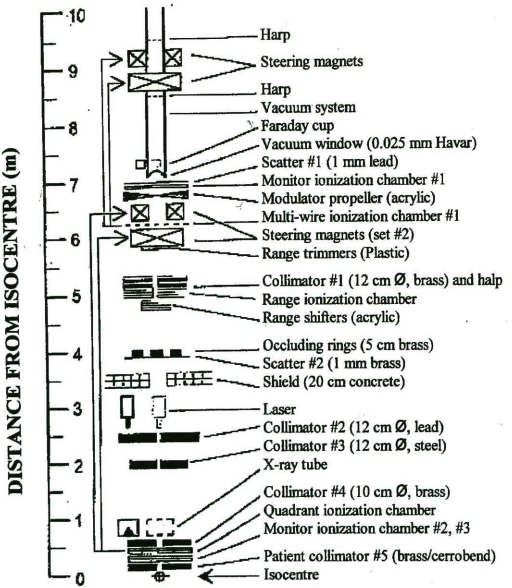


Fig 1.7.1. Layout of the 200 MeV horizontal proton therapy beam modification system. The drawing is not to scale, but all the beam line components are shown in their approximate positions

[http://www.tlabs.ac.za/public/MedicalRadiation(Protons).htm]



Fig 1.7.2. A 5cm range modulating wheel (Propeller), made of acrylic, is used to spread out the Bragg peak of the proton beam.

CHAPTER 2

2. LITERATURE REVIEW

2.1 Radiotoxicity of Protons on cells

The efficiency of producing biological damage per unit radiation dose on cells varies with radiation quality. Conventional explanations for this rely on spatial differences in the radiation track structure, and in general, there are very large temporal differences in the delivery of the radiation energy at the cellular level [Katz 1988]. For this reason radiation absorbed by cells can be classified as high-LET or low-LET. High-LET radiation normally deposits substantial amounts of energy by individual heavily ionizing tracks on a timescale of the order of picoseconds [Hill *et al.*, 2002]. By contrast, each low-LET radiation track deposits a small amount of energy. Many of these tracks, distributed over the whole cell, are then required to deliver an equivalent dose to a high-LET track and they are usually delivered over much longer timescales (typically seconds). During this time, chemical, biochemical and biological processes are occurring.

It is almost certain that DNA represents the most critical target as very short range radiation emanating outside cells are less likely to induce biological damage [Slabbert *et al.*, 1999]. However, it is likely that the nuclear membrane may be important too [Hall 1994]. When biological material absorbs any form of radiation, charged or uncharged particles, there are possibilities that it may interact directly or indirectly with the DNA of the cells [Hall 2000]. With high-LET radiation (neutrons or α-particles) there is a higher probability for direct action with the DNA of a cell while low-LET sources (X- or γ-rays) are more likely to inflict DNA damage via the formation of radical species that diffuse to

the target molecule (indirect action) (Fig 2.1.1). As a result, direct DNA damage can be associated with lethal damage and indirect actions with repairable damage (Hall 2000). The ratio of lethal to repairable damage is determined by ionization density, and in the case of protons this starts out to be very low (< 1 keV/ μm) to as high as 90 keV/ μm when protons are slowing down (Raju 1995).

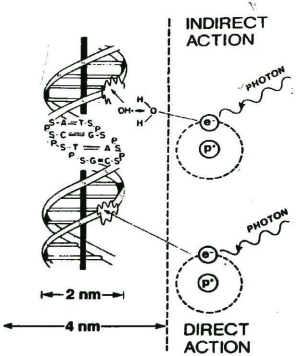


Fig 2.1.1. The direct and indirect actions of radiation with DNA in the cell. The letters S, P, A,T, G and C represent sugar, phosphorus, adenine, thymine, guanine and cytosine, respectively. [Hall 2000]

Indirect action can be modified by chemical sensitizers or protectors, and high-LET radiations produce most biological damage by direct action, which cannot be modified by chemical sensitizers and protectors [Hall 1994].

Radiation damage in cells can be quantified by looking at the initial characterization of DNA damage, micronucleus formation, apoptosis, cell survival and cell cycle phase redistribution. All of these will respond differently depending on the quality of radiation absorbed.

In a study by Green *et al.* [2000], the response of thyroid cells, organized as follicles (~ 150 thyrocytes) were compared when irradiated with either γ- irradiation (^{60}Co) or 250 MeV protons (Loma Linda Proton treatment facility). It was established that the cells treated with γ-rays were able to repair DNA damage relatively rapidly so that by 1-hour post irradiations they had ~20% less DNA damage than the same cells irradiated with protons. These results were further supported by an increased frequency of chromosomal damage as measured by the presence of micronuclei. Proton irradiation induced micronuclei at a rate of 2.4% per Gy, which at 12 Gy translated to 40% more micronuclei than in comparable γ-irradiated cultures.

The same investigators also reported apoptosis in cells irradiated with protons compared to cells exposed to γ-rays, suggesting that the damage was more severe. A difference in radiation quality is also evident when the α-components of cell survival curves are compared. This is reported by Green *et al* [2000] to be 0.05 Gy^{-1} for γ-rays and 0.12 Gy^{-1} for protons. Assessing the radiation-induced cell cycle phase redistribution they conclude that gamma radiation and protons both produced similar dose-dependent deviations towards a build-up in the G_2–phase. This is dependent on dose but not radiation quality [Green *et al.*, 2000].

DNA damage induced by high-LET radiation has been shown to be more complex than that produced by low-LET radiation, and consequently presents a greater challenge to the repair systems of the cells. This was confirmed by much more repair noted on the slopes of low-LET survival curves and less repair on that of high-LET survival curves [Schettino *et al.*, 2001].

2.2 RBE and LET relationship.

The biological effects of protons depend on their energy, therefore the LET distribution and RBE will depend on the initial beam energy and the beam shaping devices [Paganetti and Goiten 2000]. As the energy of the protons decreases from about 1000 to 1 MeV, the linear energy transfer (LET) increases from about 0.5 to 30 keV/μm. With a further decrease in proton energy, LET rises to a maximum of 90 keV/μm at 100 keV [Raju 1995].

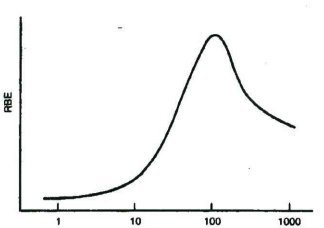


Fig 2.2.1. Generalized relationship between RBE and LET [IAEA Manual 2001].

In general, as the LET increases, the RBE increases then eventually reaches a maximum and starts decreasing. The behaviour of the RBE values (α/α_γ ratio) versus LET with C3H10T1/2 cells showed a similar RBE, with the LET ranging from 11 to 20 keV/μm, followed by a sharp rise by as much as a factor of 2.3, up to a value of 33 keV/μm [Bettega et al., 1998].

The plateau region of the Bragg curve is of a high energy hence lower LET, whilst the energy is somewhat lower in the middle of the SOBP and much lower (high LET) at the distal part [Gueulette *et al.*, 1996]

Low energy proton beams show on average the highest LET [Paganetti and Goiten 2000]. These beams also have the sharpest decrease in fluence with depth of penetration. This is true for both the modulated and the unmodulated Bragg curves. A study by Paganetti *et al* (2002) indicates that LET increases slightly throughout the SOBP and significantly at the terminal end of the SOBP.

The irradiations more distal in the SOBP of a 70 MeV beam resulted in higher chromosome aberration frequencies per unit dose [Matsubara *et al.*, 1990]. Aberration frequencies were 1.5 to 2.0 times higher than those seen for cells exposed at positions more proximal within the same broadened peak. These results could be explained by an increase in LET with depth. By comparing the change in LET with the change in aberration frequencies it appears that LET has more influence on the induction of chromosome aberrations at lower doses than at higher doses. Considering the theory of dual radiation action, a higher RBE is expected at lower doses [Kellerer and Rossi 1972].

Survival curves change shape depending on the LET. This includes an increase in the slope and a reduction in the width of the shoulder with LET. Above 30 keV/μm the survival curves are well represented by a pure exponential function ($\beta = 0$). Even a low LET proton curve of about 11 keV/μm has a slope steeper than that of γ-rays, implying that even at high energies protons are more effective than γ-rays [Bettega *et al.*, 1998].

The experimental data on a relationship between RBE and LET for mammalian cell survival with very low energy (0.76 - 3.36 MeV) protons, α particles and heavy ions is shown in (Fig 2.2.2). This graph indicates that the peak effectiveness of charged particles shifts towards lower LET values when the charge of the particle is reduced [Raju 1995]. For this reason cellular response to different energy protons is displaced to the left (Fig 2.2.2). This means that protons with the same ionization density of that of heavier particles are effective in inducing cellular damage. For example, at about 30 keV/μm the RBE for heavy ions is less than 2, whilst that for protons is more than 3.

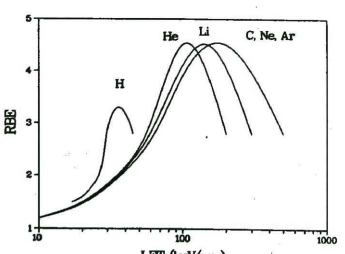


Fig 2.2.2. Schematic representation based on experimental data the relationship between RBE and LET for protons, α-particles and heavy ions [Raju M.R 1995].

The biological weighting function (RBE) for protons has been estimated by Gueulette *et al* (1996). For an unmodulated beam of 85 MeV protons this factor remains close to unity. This is not surprising since the LET spectrum overlaps that of Cobalt-60 to a very large degree (Fig 2.2.3). It is estimated for intestinal crypt regeneration that the weighting function can be as high as 4 at 100 keV/μm. However, the prevalence of ionization densities this high is very low for protons. When a proton beam is modulated higher linear energies are noted, but this overlaps with only a small part of the biological weighting function. Thus, only modest increases in beam potency can be expected.

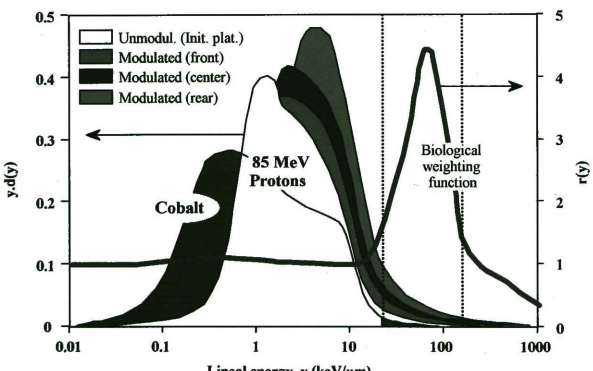


Fig 2.2.3. Microdosimetric spectra measured at different depths in the 85 MeV proton beam produced at Louvain-la-Neuve, and for ^{60}Co γ-rays. The biological weighting function r(y) for intestinal crypt regeneration has been superimposed. This function expresses the variation of RBE as a function of linear energy (y) [Gueulette et al., 1996].

Heavier ions such as boron have a depth dose curve similar in shape to that of protons but with a much shortened range in water (~ 6 mm for 460 MeV ^{10}B) [Persson *et al.*, 2002]. These investigators measured RBE values of 1.98, 2.85 and 3.37 for radiation energies of 360, 160 and 64 MeV, respectively. This corresponds to LET values of 40, 80 and 160 $eVnm^{-1}$. As the energy in the plateau region is 360 MeV for this particle beam it means that the RBE is a minimum of approximately 2, even for the highest energy.

No difference in the effectiveness of C3H10T1/2 cell inactivation for protons and deuterons with the same LET has been reported [Bettega *et al.*, 1998].

2.3 RBE variations with biological parameters

The biological endpoint used to determine radiotoxicity can affect the RBE estimated for protons.

To date a number of studies have been performed on the proton beam at Faure and in all cases RBE values greater than unity have been observed when measured with a variety of endpoints. This includes cell survival measurements, intestinal tolerance in mice after fractionated irradiations [Gueulette *et al.*, 2001], as well as late fibrosis in lung [Gueulette *et al.*, 2000]. Thus far, radiation beam quality in the last few millimeters of the spread out Bragg Peak (SOBP) has only been estimated once using cells in culture [Slabbert *et al.*, 1995]. These measurements indicated an increase in radiotoxicity by as much as 16 % relative to the plateau region. In radiotherapy, changes in the biological effective dose of greater than 10% are regarded as being of clinical significance.

Relative to ^{60}Co gamma rays, RBE values (α-proton / α-gamma) of approximately 2 have been reported for C3H10T1/2 cells irradiated with protons with LET values of between 11 and 20 keV/um [Bettega *et al.*, 1998]. This rises sharply to a value larger than 4 when the ionization density is 33 keV/ um.

Belli *et al.*, (2000) studied the inactivation of human lung fibroblasts (HF19) and human mammary epithelium tumour cells (SCC25 and SQ20B), as well as normal epithelial cells (M/10) when irradiated with 30 keV/um protons. The RBE values, with respect to ^{60}Co, range from 3.2 – 0.8. The four human cell lines, with various sensitivities to ^{60}Co γ-irradiation, show an increased RBE with cellular resistance. The RBE (2Gy γ) with the 30 keV/μm beam, evaluated as the ratio of 2 Gy to the proton dose, producing the same inactivation level as that given by 2 Gy of γ-rays, was 3.2 for SQ20B cells and 1.3 for SCC25 cells. These cell lines were derived from human epithelial tumours of the larynx and tongue, respectively. An RBE value of 1.8 is reported for M/10 cells, derived from normal human mammary epithelial, and 0.8 for HF19 cells derived from normal human lung fibroblasts.

It is important to note that an increase in the RBE of protons is seen when the proton energy is reduced. In a clinical beam the entrance energy is typically 190 – 250 MeV and this is reduced to about 10 MeV in the region of the Bragg peak [Raju 1995]. This reduction in proton energy is associated with only marginal increases in RBE. By contrast, further reductions in proton energy result in more extensive increases in RBE. For example, Perris *et al* (1986) quantified the response of V-79 cells to 7.4 and 3.0 MeV

monoenergetic proton beams. An RBE value of 1.7 was established for 7.4 MeV protons relative to ^{60}Co gamma rays and this increases to 2.8 for 3.0 MeV protons. Therefore, in the low energy proton range (10 MeV) RBE values increase substantially with decreasing proton energy.

Variations in proton RBE as a function of dose for irradiations at different positions in a 200-MeV proton beam have been shown to decrease when measured with intestinal crypt regeneration in mice [Gueulette *et al.*, 1997]. RBE values were found to continuously decrease from about 1.25 at 11 Gy to 1.05 at 14 Gy. This is for irradiations along a 7 cm SOBP. With the exception of a decrease in RBE in the middle of the SOBP, the beam increases from 1.1 in the plateau to 1.23 in the distal part of the SOBP. These investigators stated that the crypt regeneration assay appeared to be unable to reveal small RBE variations and, therefore, although an increase is found on average with depth compared to ^{60}Co γ rays, the changes are not always statistically significant.

A clear illustration of the influence of dose and depth on proton RBE has been reported for the SOBP of a 70 MeV proton beam [Wouters *et al.*, 1996]. Using V79-WNRE cells these investigators showed that there is an increase in RBE both with increasing depth and with decreasing dose. Values from approximately 1.2 at the proximal part to greater than 1.3 at the distal part of the SOBP were obtained. RBE values increase to 1.37 and 1.56 at 2 and 1 Gy, respectively. As such, the use of a single RBE value in different radiation protocols can be an oversimplification. Using a flow cytometer that allows accurate single cell sorting, these investigators also noted a substructure in the dose

response relationship, below 1.5 Gy. This points to an increase in the effectiveness of proton radiation per unit dose at high levels of cell survival. This is for irradiation in both the proximal and distal regions of the SOBP.

The study by Blomquist *et al* (1993) has confirmed that for protons, the RBE increases with depth along the beam axis. Furthermore, most studies shows that high RBE values are obtained when mutation and chromosome aberrations are used as biological endpoints instead of clonogenic cell survival [Fuhrman *et al.*, 1988 and Belli *et al.*, 1991].

A study by Paganetti *et al* (2002) with references from Wouters *et al* (1996) and Blomquist et *al* (1993) stated that for the *in vitro* data from clinical beams of 70 and 67 MeV, RBE values estimated at the centre of the SOBP ranged from 0.86 to 2.1 with a mean value of 1.22 and a standard error of 0.02. Values greater than 1.3 in the above were observed using V-79 cells. For *in vivo* studies, RBE values ranged from 0.73 to 1.55 with a mean value of 1.10 and a standard error of 0.01. Therefore, RBE values measured *in vivo* are lower and have less spread than those obtained from *in vitro* systems. Overall, both the *in vitro* and *in vivo* studies showed a statistically significant increase in RBE when lower doses per fraction were applied. This is much smaller for *in vivo* systems. The *in vitro* data in this study uses cell survival as an end point whilst the *in vivo* data uses tissue response. The *in vivo* data indicate that a generic RBE of 1.1 is reasonable for proton therapy applications [Paganetti 2003].

The experimental data published by Gerweck and Kozin (1999) also indicates that the RBE of protons increases with decreasing dose, or dose per fraction, and increasing depth in the SOBP. They indicate that the RBE is likely to be dependent on the α/β ratios of the target cells or tissue.

The 6cm SOBP of a 190 MeV per nucleon proton beam and a 320 MeV per nucleon carbon ion beam gave different RBE values using cultured human salivary gland cancer cells (HSG cells) [Kagawa *et al.*, 2002]. RBE values were calculated from the cell survival curves at the dose that would reduce cell survival to 10% (TD_{90}), values for protons ranged from 1.01 to 1.05, and from 1.23 to 2.56 for carbon ions. The regeneration of crypts per jejunal section was used as an endpoint and RBE values ranging from 1.01 to 1.08 were noted for protons, and 1.15 to 1.88 for carbon ions. Interestingly, skin response to carbon ions in the middle of the SOBP gave a value of 2.16. A 4MV X-ray beam was used as the reference radiation for this work. These results confirm a variation in the RBE with biological endpoint, even if the ionization density of the charged particle is very high.

For a given initial energy, the RBE of protons may vary significantly with the shaping of the beam and its resulting spectrum [Gueulette *et al.*, 1996]. The microdosimetric spectra measured at different depths in the 85 MeV proton beam produced at Louvain-la-Neuve showed a progressive shift in linear energy spectra towards the higher values. In the very same study, the RBE of the Chinese hamster ovary cells cultivated *in vitro* was found to be 1.11 ± 0.05 at the initial plateau of the unmodulated beam, and 1.10 ± 0.03 at the middle of a 0.5cm SOBP. Values of 1.03 ± 0.03 at the beginning of a 3cm SOBP and

1.07 ± 0.03 at the end were also found. Regenerated crypts for mice exposed in the middle of this 3cm SOBP yield an RBE of 1.08 ± 0.03. These results by Gueulette *et al* (1996) shows that there is an increase in RBE when the SOBP is smaller.

A study by Matsubara S *et al* (1990) used a 70 MeV proton beam for the induction of chromosome aberrations in peripheral lymphocytes. The frequency of chromosome aberrations at 5 mm in the unmodulated proton beam showed a similar dose-response relationship to that of ^{60}Co γ rays. However, at greater depths in the SOBP (15 and 25 mm) higher aberration frequencies were induced compared to that by γ-rays. The frequency of dicentrics and rings were analyzed for doses ranging from 0.1 to 8 Gy. For exposures at both 15 and 25 mm (SOBP) the frequency of chromosome aberrations was found to be significantly higher than that for ^{60}Co, but only at doses less than 1 Gy. The results show RBE values of 2 in the lower dose range at 15 and 25mm, around unity at higher dose levels, and no RBE at 5mm (plateau).

RBE values for a 235 MeV proton beam at the National Cancer Center Hospital East (NCCHE) at Kishiwa were measured for the plateau and middle part of a 10 cm SOBP [Ando *et al.*, 2001]. Overall, values at the middle part of the SOBP ranged from 0.98 to 1.24, using 6MV X-rays as the reference radiation. The biological systems used were mouse intestinal crypt cells that gave a low RBE of 0.98 ± 0.10, and three *in vitro* cell lines, including human squamous cell carcinoma (SCC61), human fibroblasts (NB1RGB) and V79 Chinese hamster cells, which gave values of 1.24 ± 1.30, 1.10 ± 0.25 and 1.09 ± 0.25, respectively. The investigators concluded that an RBE of 1.1 would be appropriate for this proton beam.

Calculated RBE values using biological weighting functions were considered for a proton beam with an initial energy of 250 MeV [Paganetti *et al.*, 1997]. Values estimated varied from 1.1 for early intestinal tolerance assessed by crypt regeneration in mice, to 1.35 for the inactivation of V79 cells irradiated in the G_1/S phase, and 1.25 for cells in late-S phase and inactivation followed. For the initial proton energy of 70 MeV, the values of the RBE were 1.3, 1.9 and 1.6, respectively. This study indicates the variation of the RBE with the cell cycle stages, tissue endpoint and the initial energy of the beam.

Using the survival of Chinese hamster cells (clone 431) extracted from embryo lung to quantify the RBE of a 179 MeV medical proton beam at Moscow synchrotron [Yashkin *et al.*, 1995], mean RBE values at a 37% survival level were found to be 1.10 ± 0.04 at the entry of the unmodulated beam, and 1.14 ± 0.05 in the centre of the SOBP. The gamma-radiation of ^{60}Co was used as the reference source.

It is instructive to see these proton RBE findings relative to that of heavier particles. A comparison of dose-response curves to examine the RBE of short range ^{210}Po versus 250 kVp X-rays in producing damage to cultured bovine aortic endothelial cells yielded values of 13.1 ± 2.5 for cell viability, 10.3 ± 1.0 for live cell number and 11.1 ± 3.0 for lactate dehydrogenase (LDH) activity [Thomas *et al.*, 2003]. The RBE for clonogenic survival was 14.0 ± 1.0, based on the slope of the dose-response curves, and 13.1, 9.9 and 7.7 for 50%, 10% and 1% survival rate, respectively. These investigators concluded that exposure to ^{210}Po was 7 to 14 times more effective than X-ray exposure in causing endothelial cell damage.

Comparing the difference in RBE between ^{10}B ions and ^{60}Co γ-rays for human melanoma cells using *in vitro* cell survival based on the clonogenic assay, values obtained at 10% cell survival for an energy of 40, 80 and 160 $eVnm^{-1}$ were 1.98, 2.85 and 3.37, respectively [Persson *et al.*, 2002].

From the literature review, experiments show a clear variation in RBE values with biological endpoint, dose or dose/fraction, size of the SOBP, initial energy of the beam, position along the SOBP, and materials used on the beam.

Considering the above, it is clear that data are required on proton RBE in the last few mm of a SOBP, as well as at the distal edge. This is the motivation for carrying out the study.

CHAPTER 3

3. RESEARCH MATERIALS AND METHODS

3.1 Cell storage, retrieval and culture maintenance.

In this study, *in vitro* cell culture methods were employed. For this Chinese hamster ovary cells (CHO-K1) and peripheral blood lymphocytes (T-cells) were cultivated. The latter was obtained from a single male donor and used throughout the investigation. Chinese hamster ovary cells are well established in culture in the radiobiology laboratory at iThemba LABS and identical clones are stored in liquid nitrogen.

CHO-K1 cells have a doubling time of 11 hours, grow in culture with ease and have a high plating efficiency. As such, they are suitable for cell survival studies using colony formation. These cells grow as monolayers and attach to the surface of the culture flask, as well as glass coverslips. For this reason it is convenient to study micronuclei formations using this cell type. CHO cells have well-defined nuclei and this facilitates the identification of micronuclei.

CHO-K1 cells are stored in liquid nitrogen (-197 ^{0}C) in a mixture of 10% dimethyl-sulfoxide (DMSO) and 90% cell suspension in pure foetal calf serum. DMSO is an organic solvent and acts as an anti-freeze. Aliquots of 2 ml samples in cryogenic vials are available for use. To initiate the culture, an ampoule stored in liquid nitrogen is placed directly into a 37 ^{0}C water bath to thaw. The cell suspension is then mixed with 8 ml Eagle Minimum Essential Medium (α-MEM) under sterile conditions. α-MEM is a growth medium containing all the essential vitamins, amino acids, buffer salts and

antibiotics (penicillin and streptomycin). The working solution contains 10% Foetal calf serum (FCS). The cell suspension is first centrifuged at 1000 revolutions per minute (rpm) for 10 minutes to form a cell pellet. The supernatant is decanted and the pellet re-suspended in 5ml α-MEM. This 5ml cell suspension is then seeded into a T25 tissue culture flask and incubated at 37 ^{0}C in an atmosphere of 5% CO_2. The tissue culture flask caps are loosened to allow for gaseous exchange.

Cell culture growth was monitored on a daily basis by observing the cells microscopically. This is to assess if there is any bacterial contamination or abnormalities in the cell growth. When the cells reach confluence it is necessary to detach the adherent cells by trypsinisation before sub-culturing them in new flasks.

A method of "dry" trypsinisation was followed. For this, cell monolayers are dissociated using trypsin, derived from a beef pancreas and which is a proteolitic enzyme. The process is facilitated by using EDTA mixed with trypsin. EDTA adsorbs heavy ions like Mg^{++} and Ca^{++} involved in the attachment of cells to each other and to the substrate.

The medium, which covers the monolayer of cells, is removed from the tissue culture flask. The cell monolayer is then rinsed twice with 1.5ml of trypsin-EDTA mixture, and discarded. The flask is now returned to the incubator for 3 minutes. During this time the cells detach and become spherical as a result of the enzyme. The flask is then tapped in the palm of the hand in order to further loosen the cells to yield a single cell suspension. The enzymatic action of the trypsin is halted by the foetal calf serum in the growth medium. Cell suspensions are now ready for counting, diluting or sub-culturing. All the cell culture work was carried out under sterile conditions in a laminar flow cabinet.

3.2 CHO-K1 cell preparation for survival analysis.

A haemocytometer was used to estimate the number of cells per ml in a suspension. Cell samples were diluted according to an expected level of survival after radiation treatment and seeded in 60 mm petri dishes. The aim of diluting the cells is to end up with approximately 200 colonies per petri dish to be counted with reasonable ease, irrespective of the radiation dose applied [Nkuna K.K 2001]. Before irradiation, cultures were incubated for 4 hours to allow cells to attach to the dish.

A typical dilution sequence is as follows.

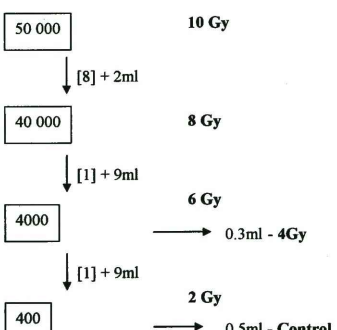


Fig 3.2.1. A schematic flow diagram showing how the cells were diluted in test tubes and then seeded in petri dishes before being irradiated. Numbers in brackets represents cell suspension volumes while the others represent that of the growth medium.

Once the cells had attached to the growth surface, the medium was removed and the monolayers irradiated at different depths along the SOBP at different doses. Samples were prepared in triplicate for each dose point. Immediately after treatment the growth medium was replaced and the samples incubated for a further 7 days in order to allow the formation of colonies (> 50 cells).

To ensure that the procedure of preparing cells for treatment had no effect on the outcome of the results, an experiment was performed to determine the influence on cells left without growth medium for 7, 15 and 30 minutes.

3.3 Staining and counting of colonies.

After a week of incubation, the medium was discarded and the colonies formed were rinsed with PBS, stained with amido-black for 30 minutes and rinsed with a fixative (3:1 v/v methanol:acetic acid). Surviving cells, observed in the form of colonies, were counted and the surviving fraction (SF) for each dose calculated as Sf = number of colonies /(number of cells seeded *plating efficiency).

3.4 CHO-K1 cell preparation for micronuclei analysis.

Samples from a single cell suspension were collected using sterile tuberculin syringes. 0.5ml of the cell suspension, with a concentration of $20x10^4$ cells/ml, were treated with various doses of radiation. The irradiated cell suspensions then pipetted into 35 mm diameter Petri dishes containing glass coverslips. The cells samples were diluted to a volume of 2 ml to give a total of 50 000 cells per dish. Cytochalasin B was added immediately after irradiation to all the samples to give a final concentration of 2 μg/ml

and samples were incubated for 24 hours. This is sufficient time to render at least 50% of the cells binucleated. The addition of this drug produces binucleate cells by permitting karyogenesis but interfering with the final stages of mitosis [IAEA Report 405, 2001].

Cell samples were fixed by first discarding the growth medium and then rinse the cover slips with PBS solution. A fixative of methanol:acetic acid (3:1 v/v) was added and left for 10 minutes. The fixative was then discarded and the cover slips dried overnight before staining.

Cover slips were processed by staining with acridine-orange for 1 minute, washed with water, and de-stained with buffer solution (pH 6.8) for another minute. A drop of buffer solution was placed on the microscope slide and the cover slip carefully mounted upside down. To prevent the preparation from drying, the coverslip edges were sealed with nail vanish.

Micronuclei scoring was restricted to binucleated cells. For this purpose a Zeiss Axioskop fluorescent microscope equipped with a FITC filter set was used. Micronuclei formed due to radiation were easily identified using a 40X objective (Fig 3.6.1).

3.5 Isolation of T-lymphocytes from whole-blood.

Whole-blood samples were collected into 4 ml vac-u-test tubes identified with a purple cap (anticoagulant EDTA). Each sample was mixed with 2 ml sterile phosphate buffered saline (PBS) and carefully layered on top of 3 ml Ficoll (Histopaque 1077) in a 10ml conical bottom plastic test-tube. The tubes were centrifuged at 1000 rpm for 30 minutes.

After centrifugation three layers were visible. The top is a serum/PBS mixture was discarded, as was the bottom layer of red blood cells.

The isolated lymphocytes taken from the buffy layer of mononuclear cells were then washed with 5 ml sterile PBS and centrifuged at 1000 rpm for 10 minutes. The supernatant was decanted and the cell pellet mixed with 5ml of RPMI-1640 medium supplemented with 15% FCS. To ensure a consistent number of cells in each of the samples, the harvest from several whole-bloods were pooled in a single tube and equal amounts used for different cultures. This was set-up in 60 x 15 mm diameter petri dishes. Just prior to irradiation the cells in the petri dishes were centrifuged at 15 000 rpm for 5 minutes and the growth medium removed using a syringe.

3.6 T-lymphocyte preparation and staining for micronuclei analysis.

Following irradiation, the growth medium (5ml) was replaced immediately and the sample gently vortexed to mix the cells. The cell suspensions were then transferred to 10 ml round bottom test tubes. To each test-tube containing a volume of 5 ml, 50 µl of phytohemagglutinin (PHA, M-Form) was added in order to stimulate the cells to divide over the next 44 hours. At this stage, 15 µg of cytochalasin-B ($C_{29}H_{37}NO_5$) was added to a final concentration of 3 µg per ml. The cultures were incubated for a further 28 hours to allow the formation of binucleated lymphoblasts.

Samples were given a hypotonic treatment in order to swell the cells. After centrifugation at 15 000 rpm for 10 minutes, all but 1 ml of the supernatant was removed and the tube contents mixed with 5ml of 75 mM of KCl whilst vortexing. Cell suspensions were then centrifuged at 8000 rpm for 8 minutes, all but 1 ml of the hypotonic solution discarded and fixed with 3:1 (v/v) methanol:acetic acid (~ 4 ml) again whilst vortexing. Samples were finally stored in the refrigerator.

For the preparation of the slides, samples from the refrigerator were centrifuged at 8000 rpm for 8 minutes. The pellet was concentrated to about 0.5ml, mixed and a drop placed on each slide to dry. At least 4 slides were prepared per dose point. Cells were stained with acridine orange solution for 1.5 – 2 min, washed in water and de-stained in a buffer solution (pH 6.8). A coverslip was mounted on the microscope slide and sealed at the edges using nail varnish. Micronuclei were observed in binucleated cells using fluorescent microscopy.

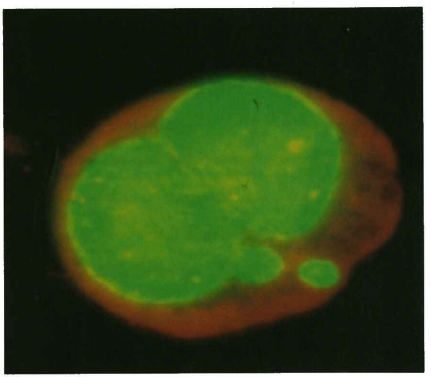


Fig 3.6.1. An example of a binucleated T-lymphocyte with two micronuclei resulting from exposure to ionizing radiation.

3.7 Proton irradiation and dosimetry.

Cell samples were irradiated at different positions along the SOBP. Blocks and slabs of various thickness of Perspex (density of 1.18 g/cm^3) were used to construct a setup with a particular depth dose. At its maximum the beam range was 210 mm of Perspex (Fig 3.7.3). Measurements were taken at the plateau (24.2 mm), middle (181.3 mm), and distal part (197.2 mm). Also, irradiations were performed at 12.4% of the maximum dose of the SOBP which is at the distal edge (207.7 mm). In all irradiations a 5cm SOBP was generated using a standard size range modulator wheel which is also constructed from Perspex. Plateau measurements were taken in an unmodulated field with a diameter of 100 mm. Immediately downstream of all samples a 48 mm thick block of Perspex was placed to serve as backscatter material.

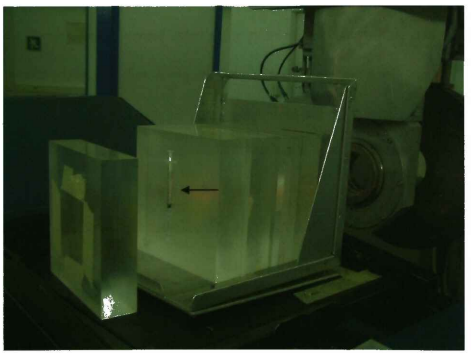


Fig 3.7.1. Experimental setup using syringes to irradiate the cells, a thick block of Perspex used as a backscatter was placed behind the syringes during the treatment.

As the proton beam is horizontal, it was necessary to discard the growth medium when irradiating cells in petri dishes.

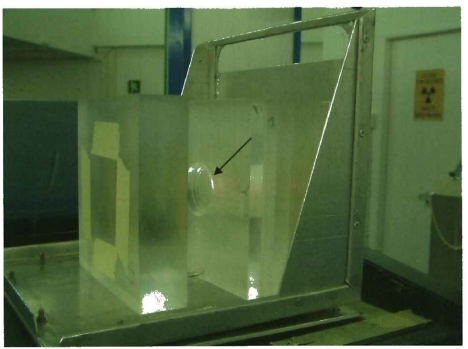


Fig 3.7.2. Proton experimental setup using petri dishes to irradiate a monolayer of cells. An arrow shows the position of the petri dish during the treatment.

The proton range specified in water is 24 ± 0.03 cm. It is recommended for an ionization chamber that the absorbed dose be measured in a phantom of water, or other materials that are close to tissue in electron density [Jones, 2001].

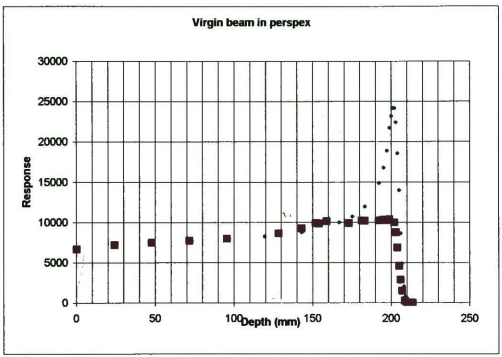


Fig 3.7.3. A 200 MeV proton beam response with depth of penetration in blocks of Perspex for the 5cm SOBP and the virgin beam.

A code of practice for clinical proton dosimetry [Vynckier S *et al.*, 1991] was followed to define the dose absorbed in each irradiation position. A Markus chamber with a build-up cap was used to measure beam output at different positions along the SOBP. An ionization chamber was placed at treatment positions for the cells and output factors were measured in monitor units per gray (mu/Gy). These were done prior to each irradiation as the values differ on a daily basis, this mainly as a result of beam energy that cannot be reproduced exactly on each day. This has particular consequences for output factors at the distal edge.

Depending on the physical dose needed at the irradiated position exposures were determined from output factors (mu/Gy) and were dialed up in a monitoring system that

automatically stops the beam. Proton dose rates differ to some extent on each experimental day but was about 3.5 Gy per minute.

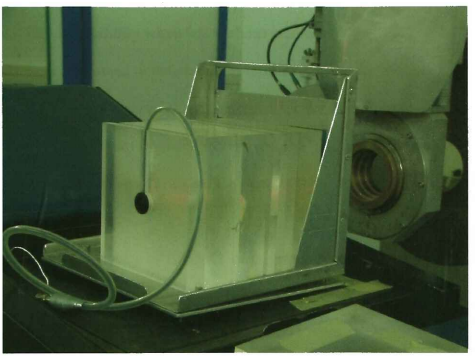


Fig 3.7.4. A Markus chamber placed at the position of irradiation to monitor the beam delivery, a thick block of Perspex serving as a backscatter was placed closely at the back of the chamber during the measurements.

3.8 ^{60}Co γ- irradiation and dosimetry

For ^{60}Co γ-irradiation, the absorbed dose was measured according to the protocol of the International Commission on Radiation Units and measurements (ICRU). The doses were delivered at a rate of 0.3 Gy per minute. Samples were positioned on a Perspex table in a 30 cm x 30 cm field. The vertical beam was directed upwards and the 5 mm thick Perspex table served as build-up material. A 50 mm thick block of Perspex was positioned immediately downstream from the cell samples and this acted as backscatter material.

CHAPTER 4

4. RESULTS AND DISCUSSION

4.1 Test of CHO-K1 viability when left without medium.

Experiments were performed to determine the influence of growth medium on monolayer cells. Tests for both cell survival and micronuclei formation were performed after removing the growth medium from cell monolayers for 7, 10 and 30 minutes (Table 4.1.1 and Table 4.1.2). The numbers shown are the mean of three tests.

Table 4.1.1. Plating efficiency of CHO-K1 cells defining cell viability after monolayers had been left with out growth medium for different time intervals. The data is compared to that of a control set of cultures.

Time (min)	Control	Test Samples	% Difference
7	70	66	4
15	73	63	10
30	79	47	32

The Plating efficiency (PE) is defined as the ratio of the number of colonies formed to the number of cells seeded. This ratio is multiplied by one hundred to give the PE as a percentage.

From these results, it is clear that cell monolayers can be left without growth medium for up to 15 minutes without significant changes in cell viability. Longer intervals, however, resulted in a loss of 32%, with respect to controls. In fact it was observed that some of the dishes left for 30 minutes were visibly dry by the time the medium was replaced. As the proton beam is located within a 2 minute walk from the cell culture laboratory, it is possible to discard the growth medium, irradiate the cells and replace the medium within 10 minutes. The maximum dose for this experiment was 10 Gy, and the dose rate for protons was 3.5 Gy/min, resulting in treatment of less than 5 minutes. The results confirmed that the method for preparing cells for experiments is workable when irradiating with protons at this Institute.

The fraction of cells becoming binucleated after 24 hours in culture serve as an indication of the cellular kinetics and, as such, reflect cell health. This experiment was also performed to look at the percentage of cells that are binucleated after removal of the growth medium for a given time. About 50 000 CHO-K1 cells were seeded in small petri dishes containing glass cover-slips. Control data are for cultures where the growth medium was present throughout.

Table 4.1.2. Binucleation levels as a function of the time for CHO-K1 cells have been left without growth medium.

Time (min)	1 Nucleus	2 Nuclei	BN Level (%)
Control	969	2913	75
7	1502	310	17
15	4	4	Too few cells

From the binucleation test data, it is clear that cells left without growth medium suffer significant biological damage. Even for a very short time interval of 7 minutes, a binucleation level of only 17% is noted compared to 75% in the control samples. This is due to the glass cover-slip which dries very quickly. For this reason it was decided not to prepare cells in this manner for proton irradiations, and that cell preparations for micronuclei analysis should be in suspension before and during irradiations. Sterile tuberculin syringes (Fig. 3.3.1) were used for this purpose and cell samples were seeded in small petri dishes only after treatment.

4.2 Survival of CHO-K1 cells after proton irradiation.

Monolayers of cells were irradiated at different positions along the SOBP to quantify their level of survival. Positions of irradiation were: the Plateau of the unmodulated beam, the distal part, and at the distal edge (12.4% maximum dose) of a 5cm SOBP.



Fig 4.2.1. An example of colonies formed after proton irradiation. In column A 200 cells were seeded and 138 survived. In columns B, C and D 4000 cells were seeded and a dose of 6 Gy given in the plateau (B), distal part of the SOBP (C) and at the distal edge with 12.4 % dose of maximum (D).

From the resulting colonies counted, the surviving fractions were calculated as follows:

S.F = [no. of colonies / (no. of cells seeded x PE)]

Table 4.2.2. The mean survival fractions and their standard deviations for CHO-K1 cells irradiated in the plateau region of the unmodulated beam (24.2 mm Perspex), distal part of the SOBP (181.3 mm Perspex) and at the distal edge (207.7 mm Perspex) corresponding to 12.4 % of the dose at maximum.

Dose (Gy)	Plateau region Mean S.F (S.D)	Distal Part Mean S.F (S.D)	Distal Edge Mean S.F (S.D)
0	1 (0)	1 (0)	1 (0)
1	0.598 (0.022)	0.502 (0.024)	0.337 (0.010)
2	0.221 (0.009)	0.175 (0.017)	0.050 (0.004)
3	0.068 (0.005)	0.043 (0.003)	0.011 (0.003)
4	0.011 (0.001)	0.007 (0.001)	0.001 (0.0002082)
5	0.005 (0.001)	0.003 (0.001)	0.00033 (0.0001155)

The mean survival fractions where normalized with respect to the plating efficiency was calculated to be 69%. In order to achieve the best results, single cell suspensions were

used for all the samples irradiated at different positions and were seeded from one cell suspension.

From the mean survival fractions, a clear decrease in the level of survival with an increase in dose was noticed at all positions of irradiation along the SOBP and the plateau of the virgin beam. It is noted that survival fractions per unit dose decrease with an increase in the position of treatment along the SOBP (Fig 4.2.3)

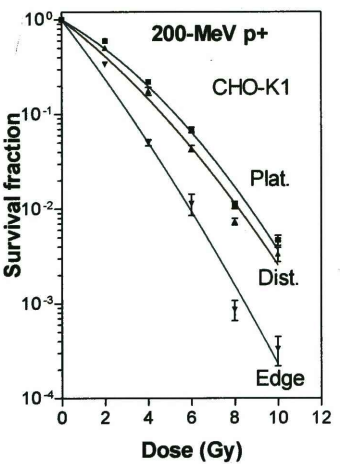


Fig 4.2.3. Survival fraction curves of CHO-K1 cells exposed to protons at different positions along the SOBP. Cells were irradiated at the Plateau (■), distal part (▲) and the distal edge (▼). Error bars indicate standard deviations.

These dose response curves were constructed by fitting the resulting data to a linear quadratic equation of the second polynomial degree using the non-linear regression analysis algorithm of the Graph Pad Prism program.

The equation used:

$$S = \exp(-\alpha D - \beta D^2),$$ where S is the surviving fraction normalized with respect to the plating efficiency, D is the proton physical dose absorbed, α is related to the induction of lethal damage and β is related to the induction of sublethal damage.

The results of the dose response curves show clear changes in radiotoxicity of the protons per unit dose at different positions along the SOBP. An increase in ionization density of the radiation is noticed as the protons travel from the plateau region (high energy and relative low dose) towards the distal part of the SOBP (low energy protons and relative high dose). These results suggest that protons are most potent per unit dose in the distal edge. Radiotoxicity is reflected by a clear difference in the slopes of dose response curves at different positions of treatment (α -value) and confirms that the result is due to changes in ionization density.

The difference in relative biological effectiveness between the irradiations in the distal part and that of the plateau is small compared to that measured at the distal edge. The RBE values calculated with respect to the plateau measurements were 1.17 for the distal part of the SOBP and 1.62 for the distal edge position (12.4% max. dose). The latter is comparable to that of neutrons that have an RBE of about 1.8 when measured with cells in culture. The biological effective dose is thus 12.4 x 1.62 = 20 %. This means, in

practice, that the relative dose in this position at the distal edge is not 12.4 % but as high as 20 % of the maximum. This has clear implications for proton therapy dose planning.

The RBE of 1.17 at the distal part of the SOBP is considered to be significant because it applies to radiation at maximum dose - last few mm of SOBP. Therefore, although the RBE is relatively small, it is likely to be of importance in radiotherapy. This observation is in line with that of proton RBE ranging from 1.0 to 1.2 (Ando K *et al.*, 2001).

This value also corresponds to the mean RBE value of 1.17 obtained from seven normal tissues and three tumours using 160 MeV clinical beam (Urano M *et al.*, 1984). In general, the observations here for the SOBP are consistent with those of other investigators using different initial proton energies and different cell types (Table 4.2.5). In particular, the RBE of 1.17 noted here with CHO cells is almost identical to that measured using V-79 cells and the same proton beam (Slabbert *et al.*, 1995).

Table 4.2.4. Survival curve parameters for CHO-K1 cells irradiated at different positions along the SOBP. The RBE is also indicated.

Position (SOBP)	α (Gy^{-1}) ± S.D	β (Gy^{-2}) ± S.D	MID ($\overline{D}$) in Gy	RBE
Plateau (Virgin beam)	0.3017 ± 0.03918	0.02592 ± 0.004644	2.452	1
Distal Part (5cm SOBP)	0.4056 ± 0.04211	0.01913 ± 0.004991	2.096	1.17
Distal Edge (12.4%)	0.6915 ± 0.06237	0.01453 ± 0.007391	1.153	1.62

For all the positions of treatment, significant α and β values were obtained. The value of α indicates the probability of lethal damage, and that of β the probability of sublethal damage. There is a clear increase in α-values and only a decrease on average in β-values with depth of treatment. This is not unusual as the larger α-values can be estimated with smaller uncertainties compared to the smaller β-values. In principle, the results suggest that as the protons penetrate tissue they become more potent by inducing more lethal damage, whilst the likelihood of sublethal damage remains constant.

The increase in ionization density at the distal edge may be due to contaminants in the beam when the protons slow down to a complete stop. This includes neutrons that are believed to play a significant role in the formation of biological damage.

The goodness of the fits (R^2) was calculated to be 0.9863 for the plateau, 0.9859 for the distal part and 0.9842 for the distal edge. As these values are close to unity they indicate relatively good fits of the dose response curves.

The mean inactivation dose value ($\overline{D}$) is a single parameter that can be use to quantify cellular sensitivity in terms of dose [Kellerer and Hug 1972]. It is a measure of the area under the survival curves. In this set of observations, the mean inactivation dose gets smaller with the increase in depth and reflects the lower survival values seen in Fig 4.2.3 and summarized in Table 4.2.4.

Table 4.2.5. Comparison of previous RBE measurements with different initial beam energies for different cell and tissues types and position along the SOBP.

Author	Beam Energy	Cell / Tissue type	Position of SOBP	RBE evaluation assay	RBE
Urano *et al.* 1984	160 MeV	Jejunum Crypts	Center (10cm)	Cell survival	1.19 ± 0.09
Urano *et al.* 1984	160 MeV	FSa – II	Center (10cm)	Cell survival	1.15 ± 0.06
Ando *et al.* 2001	235 MeV	V79	Center (10cm)	Cell survival	1.09 ± 0.25
Gueulette *et al.* 1997	200 MeV	Intestine Crypts	Distal Part (7cm)	Crypt regeneration	1.23 ± 0.03
Slabbert J.P 1995	200 MeV	V79	Distal Part (5cm)	Cell survival	1.16

4.3 Confidence ellipses for cell inactivation parameters.

Because the increase in biological damage between the plateau and the SOBP is small, it is necessary to determine the statistical significance of these observations. For this, the inactivation parameters describing the dose response curves were further analyzed in a special manner. This is based on the fact that the probabilities of lethal and sublethal damage are covariant, and this can be represented by an ellipse that marks out the 95%

confidence uncertainties of the cell survival parameters. If they do not overlap for different data sets then the increase in biological effectiveness of the protons is significant at the 95% confidence level. An overlap between confidence regions means that a single pair of inactivation parameters can be used to describe the survival curves of different irradiated positions and, as such, changes in the level of biological damage per unit dose are not significant. This type of analysis for the current data set is shown in Fig. 4.3.1

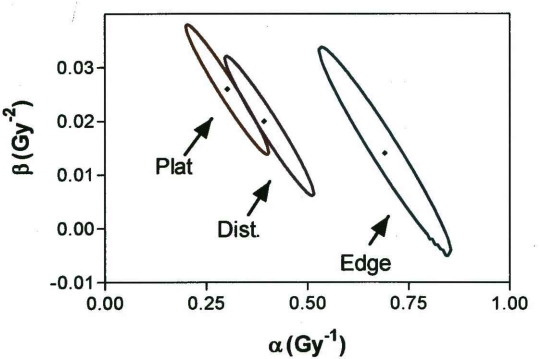


Fig 4.3.1. 95% confidence ellipses of survival data for CHO cells exposed to 200 MeV protons at different positions in the SOBP. Symbols in the middle of the ellipses indicate the best fit the respective survival curves.

The results for the distal part of the SOBP reflect a relatively small but significant increase in biological damage in response to ionization density with respect to that in the

plateau region. The RBE of 1.17 represents a meaningful increase in the radiotoxicity of the beam.

A larger increase in damage per unit dose for cells irradiated in the distal edge (12.4% max. dose) of the SOBP is evident. Again this is significant for the 95 % confidence level. Therefore, the increase in biological damage per unit dose calculated to be 62% above that of the plateau is also meaningful.

These results suggest that the expected increase in ionization density of protons as they slow down towards the distal edge translate into important variations in the biological effective dose depth profile.

4.4 Usefulness of micronuclei in CHO-K1 cells to reflect cellular damage.

Micronuclei form in cells within about 24 hours after irradiation. This is much shorter than the one week it takes cells to grow into visible colonies. The question is does micronucleus formation indeed reflect biological damage in a manner that can be used to reflect an increase in ionization density? In comparing the radiosensitivity of different cell types using neutrons and photons, it has been noted that micronuclei frequencies does not always relate to cell survival [Akudugu *et al.*, 2003].

To test the usefulness of micronuclei formations in CHO-K1 cells, two sets of measurements were first performed. First, cell samples were exposed to graded doses of ^{60}Co. One half of the samples was used to assess survival, and the other half to assess

micronucleus formation in response to low LET radiation. The same experiment was repeated using p(66)/Be neutrons to generate data for high-LET radiation. The results are summarized in Fig.'s 4.4.1 and 4.4.2.

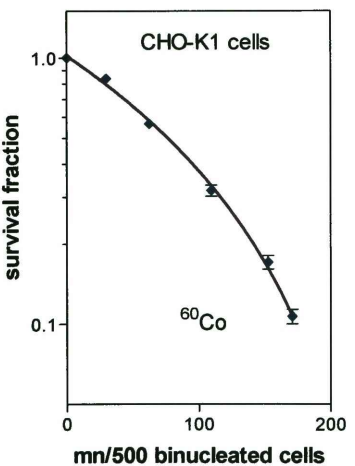


Fig 4.4.1 Surviving fractions of CHO-K1 cells exposed to gamma radiation ranging between 1 and 5 Gy and plotted as a function of micronuclei frequencies observed in each instance.

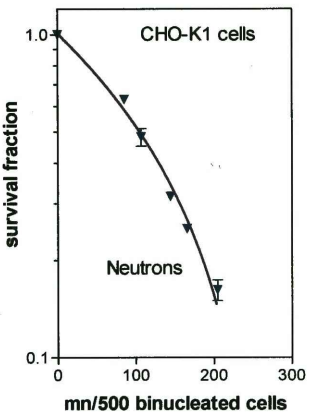


Fig 4.4.2 Surviving fractions of CHO-K1 cells exposed to p(66)/Be neutrons ranging between 0.5 and 2.5 Gy and plotted as a function of micronuclei frequencies observed in each instance.

From the data above, it is clear that cell survival decreases in a predictable manner with an increase in micronuclei frequency, and this applies to both gamma and neutron irradiation. Furthermore, it is noteworthy that both low and high-LET radiation yield similar levels of micronuclei frequencies for the same level of survival. For example, 40% survival is represented by about 100 micronuclei observed in 500 binucleated cells and this applies to both gamma and neutron irradiations. From this it is concluded that micronuclei frequencies in CHO-K1 cells are likely to reflect a true change in the biological response to radiation when the ionization density is changed.

4.5 Micronuclei frequencies in CHO-K1 cells in response to protons.

Micronuclei data for CHO-K1 cells irradiated in the plateau region of an unmodulated proton beam and at the last few millimeters (Distal Part) of a SOBP are shown in Tables 4.5.2 and 4.5.3. The interpretation of the data is somewhat complicated by the fact that poor cellular kinetics apply to all samples (Fig.4.5.1). The level of binucleation is less than 40% in all cases and less than 20% some instances. Notwithstanding this poor outcome, a further decrease in binucleation is noted with an increase in dose. This is likely the result of mitotic delay. Although the distal edge samples show, on average, less binucleation, the overall result is too poor to infer from this, increase in the biological effectiveness of the radiation.

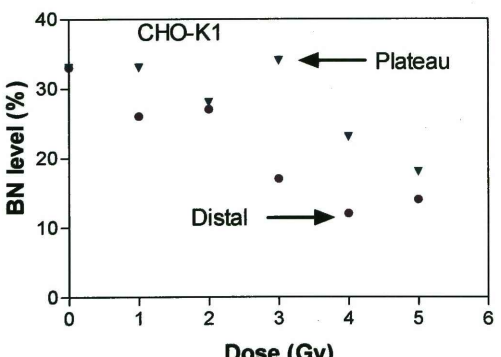


Fig 4.5.1. Percentages of the CHO-K1 cells that are binucleated for different samples irradiated in the plateau (▼) and in the distal part (●) of the SOBP.

Table 4.5.2. Micronuclei frequency observations in binucleated CHO-K1 cells and their respective binucleation levels after exposure to protons in the plateau region.

Dose (Gy)	Total # of cells	0MN	1MN	2MN	3MN	Total # of MN	MN/500	σ^2/y	μ	BN Level
0	746	735	11	0	0	11	7.37	0.987	-0.272	33%
1	745	715	30	0	0	30	20.13	0.961	-0.765	33%
2	1089	1000	87	2	0	91	41.78	0.961	-0.908	28%
3	619	547	68	4	0	76	61.39	0.984	-0.282	34%
4	322	268	46	7	1	63	97.83	1.125	1.6	23%
5	287	226	52	8	1	71	123.69	1.066	0.797	18%

Table 4.5.3. Micronuclei frequency observations in binucleated CHO-K1 cells and their respective binucleation levels after exposure to protons in the distal part of the SOBP.

Dose (Gy)	Total # of cells	0MN	1MN	2MN	3MN	Total # of MN	MN/500	σ^2/y	μ	BN Level
1	1171	1104	67	0	0	67	28.61	0.944	-1.375	26%
2	1044	953	84	3	0	90	43.10	0.981	-0.434	27%
3	1204	1031	162	11	0	184	76.41	0.968	-0.798	17%
4	1221	1009	188	23	1	237	97.05	1.026	0.647	12%
5	777	588	169	19	1	210	135.14	0.94	-1.176	14%

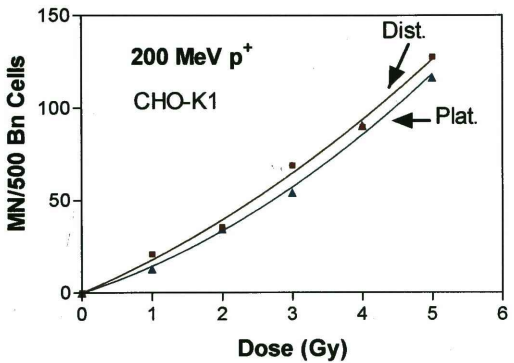


Fig 4.5.4. Dose response curve of the micronuclei frequencies observed per 500 binucleated CHO-K1 cells. Positions of treatment were the plateau (▲) of the virgin beam and distal edge (■) of the SOBP.

The mean micronuclei frequencies in this experiment show, as expected, a linear-quadratic increase as a function of dose (Fig 4.5.4). The dose response curves were generated using non-linear regression analysis and show a small increase in the biological effectiveness of the protons at the distal SOBP with respect to the plateau irradiations. An α- value of 12.14 ± 1.791 and a β- value of 2.308 ± 0.4244 was calculated for the plateau region. The values of α is 16.15 ± 2.147 and the value of β is 1.819 ± 0.509 for cells irradiated in the last few millimeters of the SOBP. The goodness of fit (R^2) values for the dose response curves are 0.9958 for the plateau and 0.9946 for the distal part of the

SOBP. An analysis of the confidence intervals of the coefficients of these dose response curves shows that the difference in the result is not significant at the 95% confidence interval (Fig 4.6.1).

The ratio of initial slope values indicates an RBE of 1.3 ($\alpha_{p+}/\alpha_{\gamma}$). This is slightly higher than the value estimated using cell survival and is to be expected since smaller doses of radiation have been used. CHO-K1 cells are, in general, relatively radiosensitive and this may result in a smaller RBE than could be estimated if a more radioresistant cell line was used [Slabbert *et al.* 1999].

When the RBE was calculated as the ratio of doses to yield the same level of micronuclei frequencies, values of between 1.07 and 1.18 were estimated. Interestingly, higher RBE values were calculated at lower micronuclei frequencies (lower doses) and smaller RBE values were noted at higher doses. This is consistent with what can be expected if the underlying cause of an increase in radiosensitivity is the result of an increase in ionization density.

This observation is, however, not supported by the respective dispersion indices of the number of micronuclei formations in different cells (Table 4.5.5). Both irradiated positions yield dispersion indices that are not significantly different from 1. This implies that the variance and the mean micronuclei frequency on average have the same magnitude.

This is expected for micronuclei formations in a low LET radiation field and, as such, can be expected when irradiating cells with high-energy protons. Even so, some increase in the σ^2/y and μ values can be expected if the increased radiotoxicity seen in the distal part of the SOBP is the result of an increase in ionization density.

Table 4.5.5. Mean dispersion index (σ^2/y) and mean standard unit normal deviation (μ) for micronuclei frequencies in CHO-K1 cells.

Position	Mean (σ^2/y)	Mean (μ)	RBE
Plateau	1.019	0.088	1
Distal Part	0.972	-0.627	1.3

4.6 Confidence ellipses of micronuclei frequency response curves.

A small increase in radiotoxicity is reflected by the dose response curves and the 95% confidence intervals of the respective curve fitting parameters shown in Fig.4.6.1.

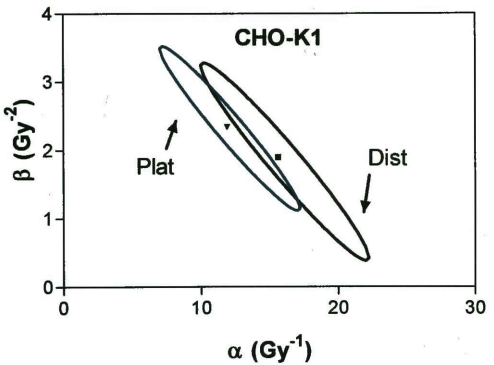


Fig 4.6.1. 95% confidence level of the micronuclei frequency data for CHO-K1 cells, following exposure in the plateau region and distal portion of the SOBP of a 200 MeV proton beam.

There is a small overlap between the ellipses indicating that a single set of curve fitting parameters can be used to describe the data of both irradiation positions. As such, at the 95% confidence level there is no significant difference between the micronuclei formation frequency per unit dose for proton exposures in these positions in the Bragg curve. Even so, a clear separation of the ellipses for the most part is noted and it likely

that significant levels of biological damage can be stated at a confidence level of 66 %. The probabilities of lethal damage are seen to be higher at the distal part when compared to the plateau, the ellipse shifts to the right giving higher α-values and this is consistent with an increase in the ionization density.

4.7 Micronuclei frequencies in T-lymphocytes

The following data Tables summarize the number of micronuclei noted in binucleated lymphocytes. Included in these Tables are the nucleation indices calculated from 300 – 400 cells with well-defined cytoplasms. The nucleation index (NI) was calculated using the number of cells containing 1,2,3 and 4 main nuclei, according to the definition by Kligerman and King (1995). The NI is the ratio of the total number of nuclei observed, divided by the total number of cells examined. A low NI (values close to 1) indicates poor lymphocyte stimulation which may be the result of cellular damage, whilst higher indices reflect a larger proportion of cells undergoing mitosis. For culture conditions used in this investigation, NI values as high as 1.9 have been observed.

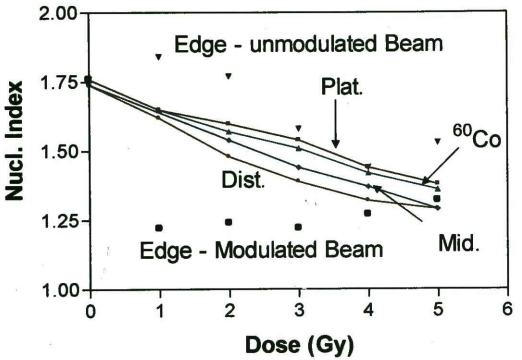


Fig 4.7.1. Nucleation indices for T-lymphocytes in response to dose absorbed at different positions in a 200 MeV proton Bragg curve. Position of irradiation were in the plateau (■) and distal edge (▼) of the unmodulated beam, also in the middle (♦), distal part (●) and distal edge (■) for the SOBP. Included are also data for exposure to ^{60}Co γ-rays (▲).

These results show that cells suffer most damage when positioned at deeper positions compare to the plateau region, and exposures to gamma rays. In the distal edge, mitotic delay was particularly prominent. This may be due to cells not being covered with growth medium during exposures. Although less cells are available for scoring, a lower nucleation index is not expected to influence the proportion of cells that form micronuclei [Kligerman and King 1995].

^{60}Co Irradiation

Table 4.7.2. Micronuclei frequency distributions observed in binucleated T-lymphocytes exposed to ^{60}Co γ-irradiation.

Dose (Gy)	Total # of cells	0MN	1MN	2MN	3MN	4MN	Total # of MN	MN/500	σ^2/y	μ	Nucl. Index
0	6045	6010	31	4	0	0	39	3.23	1.199	11.08	1.76
1	3312	3236	74	2	0	0	78	11.78	1.028	1.148	1.65
2	2473	2251	211	11	0	0	233	47.11	1.001	0.021	1.59
3	4126	3528	542	47	8	1	664	80.47	1.078	3.239	1.46
4	3906	3089	692	117	8	0	950	121.61	1.054	2.383	1.36
5	2170	1652	399	108	10	1	649	149.54	1.145	4.786	1.28

Plateau region of the virgin beam

Table 4.7.3. Micronuclei frequency distributions observed in binucleated T-lymphocytes exposed to protons in the plateau region of the unmodulated beam.

Dose (Gy)	Total # of cells	0MN	1MN	2MN	3MN	4MN	Total # of MN	MN/500	σ^2/y	μ	Nucl. Index
1	3358	3265	92	1	0	0	94	13.996	0.994	-0.246	1.65
2	4016	3675	322	19	0	0	360	44.82	1.016	0.725	1.59
3	3010	2572	388	47	3	0	491	81.56	1.065	2.537	1.53
4	1942	1591	307	41	3	0	398	102.47	1.047	1.461	1.44
5	2112	1627	391	85	9	0	588	139.20	1.103	3.351	1.38

Middle position of the SOBP

Table 4.7.4. Micronuclei frequency distributions observed in binucleated T-lymphocytes exposed to protons in the middle part of the SOBP.

Dose (Gy)	Total # of cells	0MN	1MN	2MN	3MN	4MN	Total # of MN	MN/500	σ^2/y	μ	Nucl. Index
1	1904	1744	147	13	0	0	173	45.43	1.06	1.856	1.650
2	1972	1671	283	18	0	0	319	80.88	0.952	-1.523	1.57
3	2143	1669	397	73	4	0	555	129.49	1.048	1.566	1.47
4	2190	1571	495	115	9	0	752	171.69	1.035	1.151	1.39
5	2159	1471	508	156	21	3	895	207.27	1.116	3.799	1.29

Distal position of the SOBP

Table 4.7.5. Micronuclei frequency distributions observed in binucleated T-lymphocytes exposed to protons in the Distal Part of the SOBP.

Dose (Gy)	Total # of cells	0MN	1MN	2MN	3MN	4MN	Total # of MN	MN/500	σ^2/y	μ	Nucl. Index
1	3055	2708	317	27	3	0	380	62.19	1.065	2.53	1.62
2	2021	1608	360	51	2	0	468	115.78	1.013	0.398	1.49
3	2211	1584	531	89	7	0	730	165.08	0.972	-0.943	1.39
4	2498	1591	681	191	32	3	1171	234.39	1.053	1.858	1.36
5	1644	1018	379	182	48	17	955	290.45	1.316	9.069	1.29

Distal edge of a modulated beam at 12.4 % of maximum dose

Table 4.7.6. Micronuclei frequency distributions observed in binucleated T-lymphocytes exposed to protons in the distal edge (12.4% max. dose) of the SOBP.

Dose (Gy)	Total # of cells	0MN	1MN	2MN	3MN	4MN	5MN	Total # of MN	MN/500	σ^2/y	μ	Nucl. Index
1	1830	1621	186	22	1	0	0	233	63.66	1.088	2.663	1.22
2	1612	1282	248	68	12	2	0	428	132.75	1.277	7.88	1.24
3	2091	1466	468	132	21	4	0	811	193.93	1.153	4.942	1.22
4	1992	1341	416	156	47	28	4	1001	251.26	1.507	16.01	1.32
5	1145	677	298	114	31	20	5	724	316.16	1.41	9.821	1.32

Distal edge of unmodulated beam at 12.4 % of maximum dose

Table 4.7.7. Micronuclei frequency distributions observed in binucleated T-lymphocytes exposed to protons in the distal edge (12.4% max. dose) of the virgin beam.

Dose (Gy)	Total # of cells	0MN	1MN	2MN	3MN	4MN	Total # of MN	MN/500	σ^2/y	μ	Nucl. Index
1	2760	2684	74	2	0	0	78	14.13	1.023	0.874	1.84
2	3495	3215	260	19	1	0	301	43.06	1.06	2.527	1.70
3	2348	2011	287	47	3	0	390	83.05	1.122	4.169	1.56
4	2316	1900	339	74	3	0	496	107.08	1.121	4.121	1.44
5	2464	2008	356	90	8	2	568	115.26	1.214	7.501	1.53

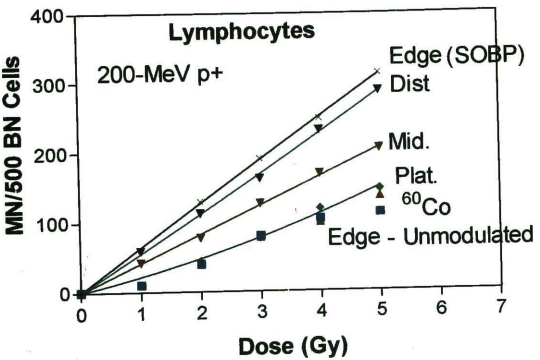


Fig 4.7.8. Dose response curves of the micronuclei frequency observed per 500 binucleated T-lymphocytes. Positions of irradiation were in the Plateau (♦) and Distal Edge (■) of the virgin beam. Position of irradiation were in the Middle (▼), Distal Part (▼) and Distal Edge (X) for the SOBP. ^{60}Co γ-irradiation (▲) is included, as well.

Goodness of the fits (R^2) for each curve were calculated, they were 0.9947 for ^{60}Co γ-rays, and 0.9984 for the middle position, 0.9986 for the distal part and 0.9995 for the distal edge position. This indicates a relatively good fit for all the positions.

From Fig. 4.7.8 it is clear that there is no difference in the rate in which biological damage develops in the plateau region, the distal edge of the unmodulated beam and ^{60}Co γ-rays. For these irradiations all data points lie on the same slope. Therefore, in terms of a change in ionization density with respect to these two treatment positions and ^{60}Co γ-rays, it is concluded that there is no observable biological difference.

By contrast, cells placed in the middle of the SOBP showed a clear increase in biological damage per unit dose and this proved to be significant at the 95% confidence interval (Fig 4.8.1). The RBE value calculated as $\alpha_{p+}/\alpha_{\gamma}$ is 2.1, and when calculated for micronuclei levels of between 150 and 30 per 500 cells, the values ranged from 1.4 to 1.9. As with the CHO-K1 cells the lymphocyte data also show an increase in RBE with a decrease in physical dose and, as such, is consistent with the notion that it is the result of an increase in ionization density. This is because the dose response curve is not only steeper but also more linear compared to the low-LET reference irradiations (plateau and cobalt-60).

The last few millimeters (Distal Part) of the SOBP show changes that are much higher than at the middle, and a dose limiting RBE value ($\alpha_{p+}/\alpha_{\gamma}$) of 2.7 was calculated. In the distal SOBP, RBE values at different levels of iso-effect ranged between 1.9 and 2.6.
In a previous analysis of this study, RBE values for CHO-K1 cells were found to be 1.3 when measured using micronuclei, and 1.2 when determined using cell survival in the distal part of the SOBP. This increased to 1.6 in the distal edge for CHO-K1 cell survival. Larger RBE values are thus noted with lymphocytes in both the distal SOBP and distal edge positions. These observations are most likely the result of lymphocytes being more radioresistant than CHO-K1 cells. The difference in inherent radioresistance has been demonstrated repeatedly by following micronuclei formations in these two cell types [Slabbert *et al.*, 1999]. The higher RBE values with radioresistance noted in this study using protons could, in fact, have been anticipated since similar observations had been made repeatedly with neutrons [Warenius *et al.*, 1984 and Slabbert *et al.*, 1996].

As a general rule, it would appear that an increase in ionization density translates into larger RBE values when the inherent resistance of cells to radiation damage is higher. This is the result of a larger variation in biological response to low-LET reference exposures and less variation to the higher-LET test irradiations. The fact that it is also seen with protons in this study is additional evidence that the change in proton beam quality is indeed the result of a change in the microscopic dose distribution of proton radiation energy.

The increase in RBE in the SOBP is of practical importance as any change in the biological effectiveness of the proton beam in this region is important because it occurs along the Bragg curve where the dose absorbed is at a maximum and is in the target treatment volume. A measure of biological effective dose that is non-uniform can thus be predicted for tumours treated with a 5 cm SOBP. This result is a consequence of an increase in ionization density with depth of treatment as an increase in the calculated α-value is noticed. β-values were again found to be not significantly different from zero, and, on average, slightly negative to yield an optimum fit. As this has no biophysical meaning, the β component was set to zero, and α values were recalculated. Even so, they were found to be significant (Table 4.7.9).

Protons in the distal edge of a modulated beam show the largest rise in RBE and this is associated with the complete slow down of these charged particles. The dose-limiting RBE value ($\alpha_{p+}/\alpha_{\gamma}$) is calculated to be 3.2 and it ranges between 2.1 and 2.6 for different micronuclei frequencies. These values must be seen in terms of how a rise in RBE influences the biological effective dose in the distal edge. Although the lymphocytes

were exposed in a position where the dose absorbed is 12.4 % of that at maximum, the biological effective dose (RBE x fractional dose) is 40%. As a result, the biological effect of dose (BED) absorbed in the distal edge is considerable higher than predicted by physical dosimetry measurements. This also implies that the effective width of the distal edge is in fact wider than the 6 mm where the physical dose drops from maximum to zero. In practice this is very important and needs to be kept in mind when planning proton therapy for lesions lying very close to critical structures, like the spinal cord, for example. To ensure that tolerance doses for such critical tissue types are not exceeded during treatment it would be advantageous to position the Bragg peak more proximal to the target volume.

Table 4.7.9. Lymphocyte micronuclei frequency parameters and their calculated RBE values at different positions along the SOBP.

Position	α (Gy^{-1}) ± S.D	β (Gy^{-2}) ± S.D	RBE ($\alpha_{p+}/\alpha_{\gamma}$)
^{60}Co γ-rays	19.86 ± 2.977	2.018 ± 0.6995	1
Middle (SOBP)	41.28 ± 0.4158	0	2.1
Distal Part (SOBP)	54.19 ± 2.440	0.6654 ± 0.578	2.7
Distal Edge (SOBP)	62.69 ± 0.3665	0	3.2

The dispersion indices (σ^2/y) for micronuclei formations in binucleated T-lymphocytes and their associated standard normal deviate values (μ values) are summarized in Table 4.7.10. For low-LET radiation a Poisson distribution of micronuclei amongst cells is expected and for this the variance (σ^2) and mean micronuclei (y) frequency is expected to be the same. As such the dispersion index (σ^2/y) should be close to 1, μ values expected to be smaller than 1.96. This is indeed observed for the ^{60}Co γ-ray, plateau and middle SOBP data.

The distal part of the SOBP shows a marginal but statistically significant increase in the dispersion index (1.08) with a μ value of 2.58. The distal edge yields a substantial increase in the dispersion index (1.23) with a μ value of 8.26.

This essentially shows that more cells formed multiple micronuclei and relatively few cells formed a single micronucleus. That is, cells are either not affected by the radiation and, if so, to a larger extent.

This is consistent with fewer particle tracks on a microscopic scale but of higher ionization density for medium irradiated with high-LET radiation. This analysis however, does not hold for the virgin beam distal edge data as a small but significant over-dispersion is noted in this case.

The mean dispersion indices at different positions

Table 4.7.10. Mean dispersion indices (σ^2/y) and mean standard unit normal deviations (μ) for micronuclei frequencies in T-lymphocytes at different positions.

Position	Mean dispersion indices (σ^2/y)	Mean standard normal deviation (μ)	Mean Nucl. Index
^{60}Co γ-rays	1.06	2.32	1.47
Distal Edge (Virgin beam)	1.108	3.84	1.61
Plateau (Virgin beam)	1.03	1.56	1.52
Middle (SOBP)	1.04	1.37	1.47
Distal Part (SOBP)	1.08	2.58	1.43
Distal Edge (SOBP)	1.23	8.26	1.26

4.8 Confidence Levels of Micronuclei Frequencies in T-lymphocytes.

Higher RBE values were noted at all depths investigated. The statistical significance of these observations are confirmed in the form of 95% confidence ellipses (Fig. 4.8.1).

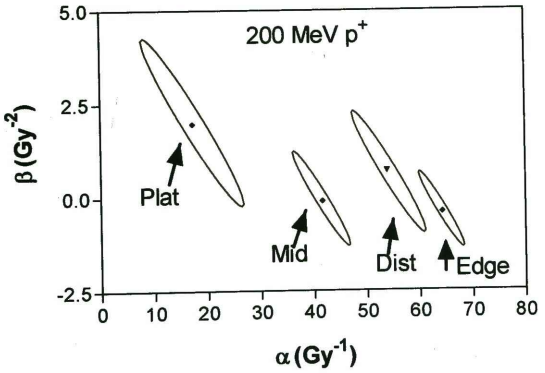


Fig 4.8.1. 95% confidence ellipses of the dose response parameters that describe the formation of micronuclei in lymphocytes.

This separation of the ellipses in Fig 4.8.1 is an indication of an increase in the biological effectiveness of protons with depth of treatment. This shows the toxicity of the protons per unit dose at different depths of penetration. The induction of lethal damage also increases with depth of treatment whereby the ellipses shift to higher α-values.

Using lymphocytes, the biological damage of protons at the distal edge is three times more effective than at the plateau region. This is comparable with that of neutrons that have an RBE of 2.6, previously noted in the research laboratory at iThemba LABS.

This increase in biological damage at the distal edge position along the SOBP is in part due to low energy protons containing a high fraction of neutrons as well as some α-particles and other contaminants. All of these contribute to the total dose absorbed. This is influenced by a series of Bragg peaks formed when a modulating wheel is introduced to form a SOBP. These peaks add up to a maximum dose (100%). Of interest here is that the distal edge of a modulated beam is also a combination of distal edges of the other small peaks. This translates to a higher ionization density in the distal edge of the modulated beam compared to that produced by an un-modulated virgin beam, as the un-modulated beam is formed by a single Bragg curve.

4.9 RBE variations with dose.

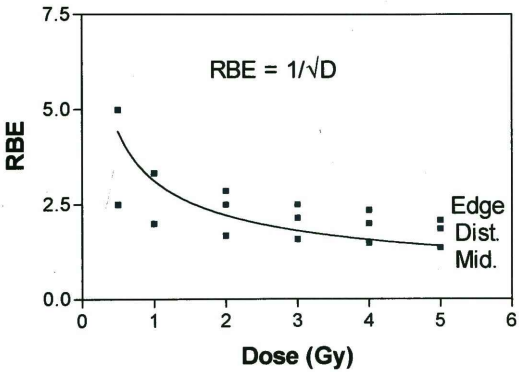


Fig 4.9.1. RBE response per unit dose of protons absorbed at different positions along the SOBP.

The RBE variations with dose are shown in Fig 4.9.1. From this it is clear that the RBE increases with a decrease in dose. The fitted line in Fig 4.9.1 indicates the change in RBE with the inverse of the square root of the dose. This was to see how experimental observations relate to an increase in RBE, based on what can be expected assuming a linear-quadratic response. This model describes the RBE variations reasonably well and is further confirmation that the increased radiotoxicity of protons noted in this study is the result of a higher ionization density.

CHAPTER 5

5. CONCLUSIONS AND RECOMMENDATIONS.

5.1 Conclusions and Recommendations.

Because of the change in LET and with energy of the protons at depth of treatment, it was hypothesized that the relative biological effectiveness of this treatment modality would not be the same for normal and tumour treatment volumes. In all cases investigated along the SOBP, using different biological endpoints (cell survival and micronuclei frequencies) for quality beam measurements, an increase in radiotoxicity with depth of treatment was repeatedly observed. Proton biological damage is more severe per unit dose further along the Bragg curve.

In this study, the RBE was shown to increase with a decrease in absorbed dose. Also, the RBE of protons varied with biological endpoint and cell type. Using micronuclei frequencies as a measure of biological damage, higher frequencies were noted for T-lymphocytes compared to that in CHO-K1 cells. The RBE changes with radioresistance.

From the results of both the CHO-K1 survival and T-lymphocyte micronuclei formation measured at the distal edge (12.4% max. dose), it was concluded that higher RBE values obtained in this position were due to low energy protons containing a higher fraction of neutrons and some other high-LET secondary charged particles. All of these contributed to the total dose absorbed at the distal edge when the protons slowed down to a complete stop. From these results it is recommended that an RBE value slightly larger than 1.1 should be adopted for the 200 MeV iThemba LABS clinical proton beam. Also, because

of the increased effectiveness of the protons at the distal edge, the dose absorbed was higher than predicted by dosimetric measurements. Therefore, for treatment planning, this position should be placed well inside the tumor treatment volume to compensate for the less steeper biological effective dose curve.

A change in the modulator wheel design is recommended that will compensate for the increased radiosensitivity with depth. This design should ensure a progressive reduction in dose absorbed along the SOBP so as to yield a uniform biological effective dose in the treatment volume.

In this study, using cell survival measurements, an increase in proton effectiveness by as much as 62% at the distal edge (12.4% max. dose) was measured. Previously, a 45% increase at 32% maximum dose was measured (Slabbert *et al.*, 1995). Therefore, higher RBE values are expected towards zero dose, and it is important to measure RBE values closer to the point at which protons come to a complete stop. Also, it would be of interest to consider additional measurements in the distal edge of the unmodulated beam.

REFERENCES:

Akudugu J M, Slabbert J P, Serafin A and Bohm L (2000). Frequency of radiation-induced micronuclei in neuronal cells does not correlate with clonogenic survival. Radiation Research. 153, 62 – 67.

Ando K, Furusawa Y, Suzuki M et al (2001). Relative biological effectiveness of the 235 MeV proton beams at the national cancer center hospital east. Radiation Research. 42, 79 – 89.

Belli M, Bettega D, Calzolari P et al (2000). Inactivation of human normal and tumor cells irradiated with low energy protons. Int. J. Radiat. Biol. 76, 6, 831 – 839.

Belli M, Ceras F, Cherubini R, Ianzini F et al (1991). Mutation induction and RBE-LET relationship of low-energy protons in V-79 cells. Int. J. Radiat. Biol. 59, No 2, 459 – 465.

Bettega D, Birattari C, Bombana M et al (1979). Relative biological effectiveness for protons of energies up to 31 MeV. Radiation Research. 77, 85 – 97.

Bettega D, Calzolari P, Marchesini R et al (1998). Inactivation of C3H10$T_{1/2}$ cells by low energy protons and deuterons. Int. J. Radiat. Biol. 73, (3), 303 – 309.

Bettega D, Dubini S, Furman Conti A M, Pelucchi T and Tallone Lombardi L (1981). Chromosome aberrations induced by protons up to 31 MeV in cultured human cells. Radiat. Environ. Biophys. 19, 19 – 100.

Blomquist E, K R Russell, Bo Stenerlow, A Monterlius, E Grusell, J Carlsson (1993). Relative biological effectiveness of intermediate energy protons. Comparison with ^{60}Co gamma-radiation using two cell lines. Radiotherapy and Oncology. 28, 44 – 51.

Chadwick R F and Leenhouts H P (1981). The molecular theory of radiation biology. (Monographs on theoretical and applied genetics; v. 5.) Pg 182.

Fowler JF (1981). Nuclear particles in cancer treatment. Medical Physics handbooks 8. 131-134. Published by Adam Hilger Ltd.

Freshney R I (1983). Culture of animal cells, A manual of basic techniques. Alan R. Liss., publishers.

Fuhrman Conti A M, Francone G, Volonte M and Gallini R E (1988). Induction of 8-azaguanine resistant mutants in human cultured cells exposed to 31 MeV protons. Int. J. Radiat. Biol. 53, (3), 467 – 476.

Gerweck LE, SV Kozin (1999). Relative biological effectiveness of proton beams in clinical therapy. Radiotherapy and Oncology. 50, 135 – 142.

Green L.M, Murray D.K, Tran D.T et al (2000). Response of thyroid follicular cells to gamma irradiation compared to proton irradiation. I. Initial characterization of DNA damage, micronucleus formation, apoptosis, cell survival, and cell cycle phase redistribution. Radiation Research. 155, (1), 32 – 42.

Gueulette J, Gregoire V, Octave-Prignot M, Wambersie A (1996). Measurements of Radiobiological Effectiveness in the 85-MeV Proton beam produced at the cyclotron CYCLONE of Louvain-la-Neuve, Belgium. Radiation Research. 145, 70 – 74.

Gueulette J, L Bohm et al (1997). RBE variation as a function of depth in the 200-MeV proton beam at the National Accelerator Center at Faure (South Africa). Radiotherapy and Oncology. 42, 303 – 309.

Gueulette J, Slabbert JP, Bohm et al (2000). Proton relative biological effectiveness for survival in mice after thoracic irradiations with fractionated doses. Int. J. Radiat Oncol. Biol. Phys. 4, 1051 – 1058.

Gueulette J, Slabbert JP, Bohm et al. (2001). Proton RBE for intestinal tolerance in mice after fractionated irradiation. Radiotherapy and Oncology. 61, 177 – 184.

Hall E J, Fifth edition (2000). Radiobiology for Radiologist.

Hill M.A, Stevens D.L, Marsden S.J et al (2002). Is the increased relative biological effectiveness of high-LET particles due to spatial or temporal effects? Characterization and OER in V79-4 cells. Phys. Med. Biol. 47, 3543 – 3555.

International Atomic Energy Agency (IAEA), Vienna 2001. Cytogenetic analysis for radiation dose assessment. A Manual.

International Commission on Radiation Units and Measurements (ICRU Report 49). Stopping powers and ranges for protons and alpha particles.

Joksic G, Pajovic S B, Stankovic M et al (2000). Chromosome aberrations, micronuclei, and activity of superoxide dismutases in human lymphocytes after irradiation in vitro. Cell Mol Life Sci. 57, (5), 842 – 850.

Jones B and Dale R.G (2000). Estimation of optimum dose per fraction for high LET radiations: implications for proton radiotherapy. Int. J. Radiat. Oncol. Biol. Phys. 48, (5), 1549 – 1557.

Jones D.T.L (2001). Reference dosimetry for fast neutron and proton therapy. Radiochim. Acta 89, 279 – 287.

Kagwa K, Murakami M, Hishikawa Y et al (2002). Preclinical biological assessment of proton and carbon ion beams at Hygo ion beam medical center. Int. J. Radiat Oncol. Biol. Phys. 54, (3), 928 – 938.

Kajioka E H, Andres M L, Li J et al (2000). Acute effects of whole-body proton irradiation on the immune system of the mouse. Radiation Research. 153, (5), Pt 1, 587 – 594.

Katz R (1988). Radiobiological modeling based on track structure. Quantitative mathematical models in radiation biology (Springer, New York), 57 – 83.

Keller A.M. and Hug. O (1972). A theory of dose-effect relations. Encyclopaedia of medical radiology. Publ. Springer, Berlin 3, 1 – 42.

Kellerer A.M. and Rossi H.H. (1972). The theory of dual radiation action. Current Topics in Radiation Research Quarterly. 8, 85 – 158.

Kligerman A D and King S C (1995). Frequency of micronucleated-binucleated lymphocytes is not significantly affected by the harvest time following G_0 exposures to X-radiation. Int. J. Radiat. Biol., 68, (1), 19 – 23.

Laitano RF and Rosetti M (2000). Proton stopping powers averaged over beam energy spectra. Phys. Med. Biol. 45, 3025 – 3043.

Matsubara S, Ohara H, Hiraoka T et al (1990). Chromosome aberration frequencies produced by a 70 MeV Proton beam. Radiation Research. 123, 182 – 191.

Mognato M, Bortoltto E, Ferrato P et al (2003). Genetic damage induced by in vitro irradiation of human G_0 lymphocytes with low energy protons (28 keV/microm): HPRT mutations and chromosome aberrations. Radiation Research. 160, (1), 52 – 60.

Moiseenko V.V, Battista J.J, Hill R.P et al (2000). In-Field and Out-Of-Field effects in partial volume lung irradiation in rodents: Possible correlation between early DNA damage and functional endpoints. Int. J. Radiat. Oncol. Biol. Phys. 48, (5), 1539 – 1548.

NAC/AR, p85-86. 1994. National Accelerator Center Annual Reports. Republic of South Africa.

Nkuna K.K 2001. Bromo-Deoxyuridene as a sensitizer of cellular damage for neutron radiation. M.Sc Thesis, University of North-West.

Paganetti H (2003). Significance and implementation of RBE variations in proton beam therapy. Technol Cancer Res. Treat. 2, No 5, 413 – 426.

Paganetti H and Goiten M (2000). Radiobiological significance of beamline dependent proton energy distributions in a spread-out Bragg peak. Medical Physics. 27, No 5, 1119 – 1126.

Paganetti H, Gerweck L E, Goiten M (2000). The general relation between tissue response to X-radiation (alpha/beta-values) and the relative biological effectiveness (RBE) of protons: prediction by the Katz track-structure model. Int. J. Radiat. Biol. 76, No 7, 985 – 998.

Paganetti H, Niemierko A, Ancukiewicz M et al (2002). Relative biological effectiveness (RBE) values for proton beam therapy. Int. J. Radiat Oncol. Biol. Phys. 53, No 2, 407 – 421.

Perris A, Paloglou P, Katsanos A A and Sideris E G (1986). Biological effectiveness of low energy protons. I. Survival of Chinese hamster cells. Int. J. Radiat. Biol. 50, No 6, 1093 – 1101.

Persson L.M, Edgren M.R, Stenerlow B et al (2002). Relative biological effectiveness of boron ions on human melanoma cells. Int. J. Radiat. Biol. 78, No 8, 743 – 748.

Raju M.R (1995). Proton Radiobiology, Radiosurgery and Radiotherapy. Int. J. Radiat Biol. 67, No.3, 237 – 259.

Ristic-Fira A, Nikolic D, Petrovic I et al (2001). The late effects of proton irradiation on cell growth, cell cycle arrest and apoptosis in a human melanoma cell line. J Exp Clin Cancer Res. 20, No 1, 135 – 143.

Schettino G, Folkard M, Prise K.M et al (2001). Low-Dose hypersensitivity in Chinese hamster V79 cells targeted with counted protons using a charged-particle microbeam. Radiation Research. 156, (5), 526 – 534.

Sgura A, Antoccia A, Cherubini R et al (2000). Micronuclei, CREST-positive micronuclei and cell inactivation induced in Chinese hamster cells by radiation with different quality. Int. J. Radiat. Biol. 76, No 3, 367 – 374.

Skarsgard L.D (1998). Radiobiology with heavy charged particles: a historical review. Phys Med. 14, suppl 1: 1 – 19.

Slabbert et al (1995). Relative biological effectiveness of 66 MeV and 200 MeV protons measured with V-79 cells. Particle therapy co-operation group (PTCOG) meeting 1995, Cape Town.

Slabbert J.P, Jones D.T.L, Schreuder N et al (1994). Variation in biological effectiveness with depth in a 200 MeV proton beam. NAC Annual reports, Pg 103 – 106.

Slabbert J.P, Langehoven J.H, Smit B.S (1999). Synthesis of [^{123}I] iodoantipyrine to study the high-LET characteristics of Auger electrons in mammalian cells. Journal of Radioanalytical and Nuclear Chemistry. 240, No 2, 505 – 508.

Slabbert J.P, Theron T, Serafin A et al (1996). Radiosensitivity variations in human tumor cell lines exposed in-vitro to p(66)/Be neutrons or ^{60}Co γ-rays. Strahlentherapie und Onkologie. 172, No 10, 567 – 572.

Slabbert J.P, Theron T, Zolzer F, Streffer C and Bohm L (2000). A comparison of the potential therapeutic gain of p(66)/Be neutrons and d(14)/Be neutrons. Int. J. Radiat. Oncol. Biol. Phys. 47, No 4, 1059 – 1065.

Steel Gordon (1997). Basic clinical Radiobiology. Second edition. Arnold publications and co-published by Oxford university press, Inc. (USA).

Thomas P.A, Tracy B.L, Ping T, Wickstrom M, Sidhu N and Hiebert L (2003). Relative biological effectiveness (RBE) of ^{210}Po alpha-particles versus X-rays on lethality in bovine endothelial cells. Int. J. Radiat. Biol. 79, No 2, 107 – 118.

Tubiana M, Dutreix J, Wambersie A, translated by Bewley D.R (1990). Introduction to Radiobiology. Taylor and Francis publication.

Urano M, Verhey L J, Goiten M, Tepper J, Suit H D et al (1984). Relative biological effectiveness of modulated proton beams in various murine tissues. Int. J. Radiat. Oncol. Biol. Phys. 10, 509 – 514.

Vynckier S, Bonnett D, Jones D.T.L (1991). Code of practice for clinical proton dosimetry. Radiotherapy and Oncology. 20, 53 – 63.

Wambersie A, Menzel H.G, Gabauer R.A et al (2002). Biological weighting of absorbed dose in radiation therapy. Nuclear technology publishing. 99, No 1-4, 445 – 452.

Warenius H.M, Britten R.A, Browning P.G, Morton I.E and Peacock J.H (1994). Identification of human in vitro cell lines with greater intrinsic cellular radiosensitivity to 62.5 MeV ($p \rightarrow Be^{+}$) neutrons than 4 MeV photons. Int. J. Radiat. Oncol. Biol. Phys. 28, 913 – 920.

Wouters B.G, Lam G.K.Y, Oelfke U et al (1996). Measurements of RBE of the 70 Mev proton beam at TRIUMF using Chinese hamster V-79 cells and the high-precision cell sorter assay. Radiation Research, 146, 159 – 170.

Yashkin P.N, Silin D.I, Zolotov V.A et al (1995). Relative biological effectiveness of protons medical beam at Moscow synchrotron determined by the Chinese hamster cells assay. Int. J. Radiat. Oncol. Biol. Phys. 31, No 3, 535 – 540.